[American Journal of Science, Vol. 307, November, 2007, P. 1096–1125, DOI 10.2475/09.2007.03]

# FLUID HISTORY DURING DEEP BURIAL AND EXHUMATION OF OIL-BEARING VOLCANICS, HERCYNIAN BELT OF SOUTHERN BRITTANY, FRANCE

FLORENCE LE HÉBEL*,§,†, SERGE FOURCADE*, MARIE-CHRISTINE BOIRON**, MICHEL CATHELINEAU**, RAMON CAPDEVILA*, and DENIS GAPAIS*

**ABSTRACT. In southern Brittany (France), the Porphyroid nappe, a Variscan tectonic unit made of volcanic pyroclastic deposits that was involved in a low-temperature/high-pressure prograde metamorphic path followed by exhumation and extension, displays evidence for very large and distributed strains achieved through dissolution/crystallization processes. Such distributed strains at low temperature are rather unusual in felsic lithologies. Recent studies have documented that these rocks deformed within a system closed to fluids. This paper presents results of detailed analyses of fluid inclusions and stable isotopes within the deformed metavolcanics and their undeformed counterparts in order to document the fluid history of the tectonic unit. Results show that its initial thermal evolution, likely occurring in a context of basin inversion, involved important open-system alteration, with K-metasomatism (adularization), oil impregnation and hydration. During the subsequent tectonic evolution, the fluids maintained a constant composition in the C-H-O-N system within the Porphyroid nappe and its para-autochthon, being water-rich and containing hydrocarbon components likely related to oil pyrolysis/oxidation. Atoll-like fluid inclusion morphology and rare undisturbed fluid inclusions with steep isochore slopes are consistent (> 750 MPa) with pressures estimated for the peak of metamorphism using mineral solid-solution thermodynamics. Fluid inclusions indicate a sub-isothermal retrograde path (between 420 and 300°C) followed by a high thermal gradient at the end of the retrograde path. Within the underlying para-autochthonous unit, only the late, high-temperature gradient is recorded by fluid inclusions. The sub-isothermal low-grade path suggests fast exhumation of the unit, without thermal relaxation. The high geotherm observed at the end of the P-T path is consistent with the post-thickening extensional collapse and associated intrusion of granites documented in the area. Hydration and heterogeneous oil/water distribution achieved in the early metasomatic evolution of the porous pyroclastic deposits are responsible for subsequent fluid confining in the Porphyroid nappe and for its strongly distributed strain pattern.**

## INTRODUCTION

During the last four decades, a considerable amount of work has enlightened our understanding of the complex interplay among fluids, mass transfer, metamorphic conditions, and strain localization, through a number of different approaches including field, (micro)structural, geochemical, fluid inclusion, experimental, and theoretical studies. Examples documenting isochemical or non-isochemical behavior, open or closed fluid systems, and channeled or pervasive deformation have been discussed (see Ferry, 1994 and Oliver, 1996, for a review). Interactions between deformation and fluid circulation are bracketed by two end-member situations: i) systems closed to fluids, either in non-fractured or in fractured rocks or ii) systems open to fluids, as classically observed within faults and shear zones (example, Fyfe and others, 1978; Kyser and Kerrich, 1990; Baumgartner and Valley, 2001, for references). In felsic lithologies, moderate temperature deformation is generally associated with strain softening and

*UMR 6118 Géosciences Rennes, Université de Rennes 1, Campus de Beaulieu, 35042 Rennes Cédex, France

**UMR G2R CNRS 7566 G2R and CREGU, BP 23, 545001 Vandoeuvre-les-Nancy cedex, France

§Present address: Université de Lyon I, ENS-LSH, UMR ICAR, BP 7000, 69342 Lyon Cedex 07, France; E-mail: Florence.le-hebel@ens-lsh.fr

†Corresponding author: F. Le Hébel

strain localization, in particular marked by the breakdown of feldspar into mica that attests to fluid channeling along shear zones (example, White and Knipe, 1978; Gapais, 1989; Dipple and Ferry, 1992; Wintsch and others, 1995; Gueydan and others, 2003).

In South Brittany (western France), the Porphyroid nappe, one of the main tectonic units of the Variscan belt of western France constitutes a remarkable exception to this rather general behavior (Le Hébel and others, 2000, 2002a). This unit, made of felsic lithologies, experienced very large penetrative strains accommodated by low-temperature dissolution-crystallization processes. Dissolution-recrystallization involved quartz and feldspars and led to the pervasive development of syn-kinematic quartz-feldspar veins. This unit experienced a high pressure, low temperature (HP/LT) metamorphic path (peak conditions: 350 ± 50°C and 800 ± 100 MPa) (Le Hébel and others, 2002b) before being exhumed during the Lower Carboniferous, prior to syn-convergence Upper Carboniferous extension (Gapais and others, 1993). This complex tectonic history was associated with low fluid mobility (Le Hébel and others, 2000, 2002a) which made the Porphyroid nappe attractive to understand how very large pervasive strains could have been achieved over thicknesses of kilometer size at such low temperatures. In addition, some of the rocks belonging to the Porphyroid nappe were recently recognized as having been impregnated with oil before deformation (Le Hébel, ms, 2002). The influence of such an uncommon pore fluid on deformation mechanisms in HP/LT conditions is to date poorly constrained.

A petrological, geochemical, stable isotope and fluid inclusion study was performed on felsic volcanics from the Porphyroid nappe and its underlying para-autochthonous counterpart in order i) to establish the fluid characteristics during diagenesis and subsequent metamorphism associated with burial and exhumation, and ii) to examine interaction between fluids and deformation mechanisms. In addition, the fluid inclusion study provided some new insight on the HP-LT metamorphic history that was independently estimated using a thermodynamical approach (Le Hébel and others, 2002b).

## STRUCTURE, PETROLOGY AND CHEMICAL COMPOSITION

### *General Situation*

The South Armorican domain (fig. 1) belongs to the internal part of the Hercynian belt of Western Europe. It is bounded to the north by the South Armorican Shear Zone, a crustal-scale dextral wrench zone. To the south, it is covered by the Mesozoic sediments of the Aquitaine Basin. The area shows two main groups of tectonic and metamorphic units (fig. 1). Lower units were affected by a Barrovian-type metamorphism (Audren and Triboulet, 1993) with an increase in grade with depth (Goujou, ms, 1992). Partial melting is widespread in the lowermost part of the pile (Jones and Brown, 1990). Peak metamorphic conditions are estimated younger than 325 Ma in Vendée (Goujou, ms, 1992), and around 320 to 310 in the Vilaine estuary and Golfe du Morbihan areas (Brown and Dallmeyer, 1996) (fig. 1). In the latter area, radiometric data on monazite (U/Pb), hornblende and muscovite ($^{39}Ar$–$^{40}Ar$), biotite (Rb/Sr), and apatite (fission tracks) indicate a rapid cooling during the Upper Carboniferous (see Gapais and others, 1993; Brown and Dallmeyer, 1996, and references therein). Gapais and others (1993) and Cagnard and others (2004) have argued that deformations observed within this lower group mainly reflect crustal-scale extension following thermal re-equilibration of the thickened crust. Sheets of two-mica leucogranites mark the top of the metamorphic pile (figs. 1B and 1C). Where deformed, the leucogranites show widespread S-C fabrics attesting to normal shearing (Gapais and others, 1993). Ages available on these granites (Rb-Sr whole rock and

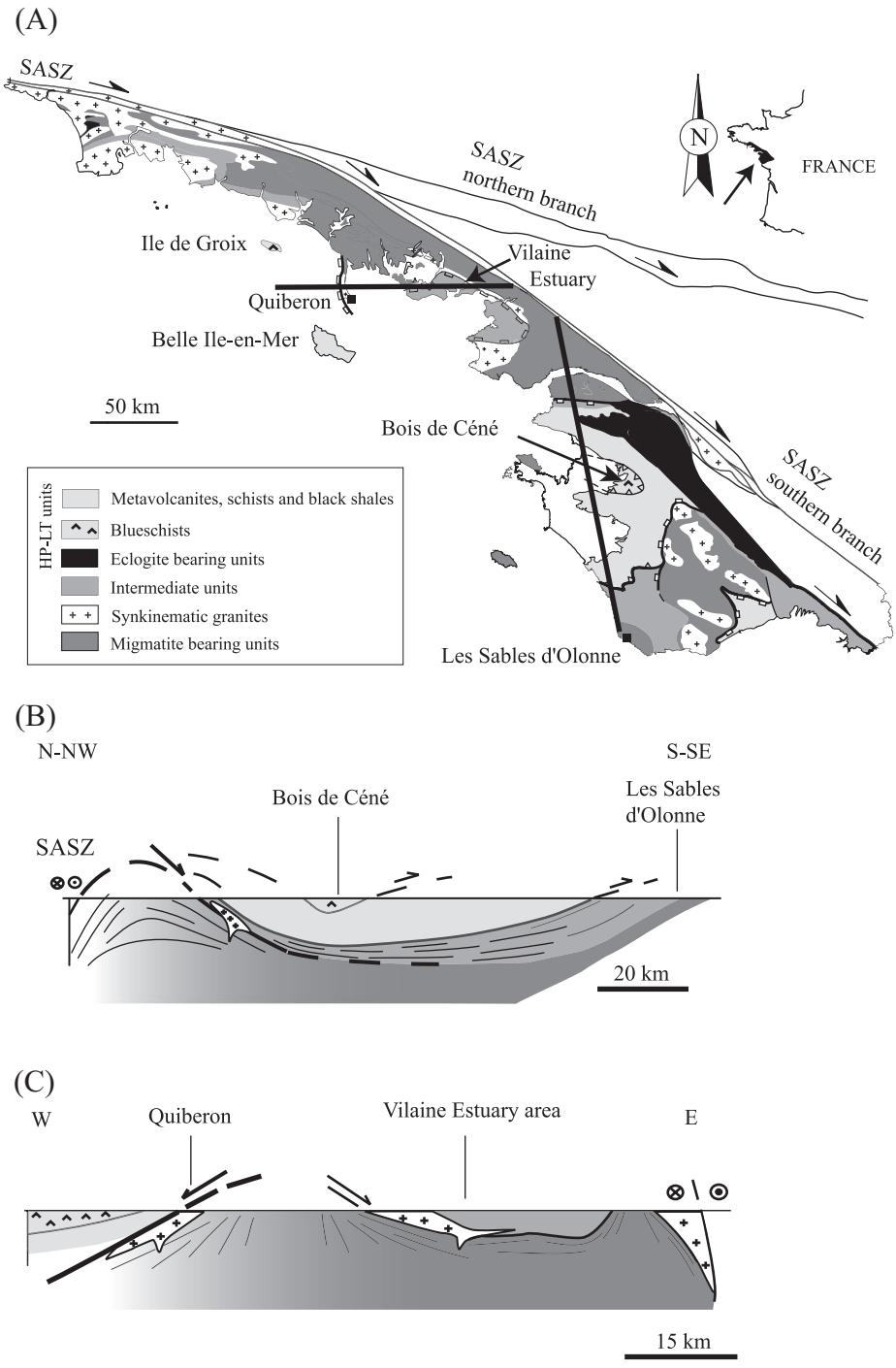


Fig. 1. Simplified geological map of the south Armorican domain of France (A) and examples of cross-sections (B, C). SASZ, South Armorican Shear Zone. Modified after Cagnard and others (2004).

$^{39}Ar$-$^{40}Ar$ on mica) range between ca. 310 and 300 Ma (Bernard-Griffiths and others, 1985; Ruffet, personal communication).

The upper group of units is marked by metamorphic histories of HP-LT type. Uppermost units consist of blueschists (Ile-de-Groix and Bois-de-Céné klippen), with peak pressures around 1.4 to 1.8 GPa for temperatures of 500 to 550°C (Bosse and others, 2002). The HP metamorphic event occurred around 370 to 360 Ma, and $^{39}Ar$–$^{40}Ar$ ages on phengite indicate that the exhumation of the blueschists occurred ca. 350 Ma (Bosse and others, 2005). Blueschists are underlain by felsic metavolcanics and metasediments from the Porphyroid nappe. Along the Vendée coast, in the Brétignolles area, the Porphyroid nappe is thrust over low-grade metasediments (Iglesias and Brun, 1976; Vauchez and others, 1987) (fig. 1B). On the other hand, in other places like the Quiberon area, the basal contact of the nappe consists of normal shear zones marked out by Upper-Carboniferous leucogranites (Gapais and others, 1993) (fig. 1C). The base of the Porphyroid nappe should thus be regarded as a thrust system related to early exhumation of HP-LT units during collision and locally cut by late extension shear zones. At the regional scale, the overall structural pattern is that of lower-crustal, migmatite-cored, extensional domes covered by HP-type units where evidence of earlier thrust-related thickening is preserved.

### *The Felsic Metavolcanics*

The Porphyroid nappe crops out from Belle-Ile-En-Mer to the Vendée area, over ca. 150 km along the belt (fig. 2). It consists of *felsic metavolcanics*, mainly meta-ignimbrites and volcanic tuffs (Ters, 1972), and of *black shales* ("schistes de St Gilles"). Among the felsic metavolcanics, porphyritic rocks *("Porphyroids")* from the nappe are foliated leucocratic gneisses characterized by stretched K-feldspar (up to 1.5 cm in size), quartz and rare plagioclase porphyroclasts embedded in a fine-grained matrix (80 to 60% of the rock) made of Qtz + Kfs + Phe ± Ab (abbreviations according to Kretz, 1983). In a few samples, scarce crystals of lightened or green biotite, of stilpnomelane and of garnet may be found. Accessory minerals are minute amounts of carbonates and rare broken apatite and zircon grains. Porphyroclasts are generally truncated, quartz and feldspar fibers filling the spaces between fragments (fig. 3C). Where preserved, euhedral monoclinic K-feldspar crystals are white-, pink- (hematite dust) or black-colored (dust made of a poorly-organized graphitic compound which will be referred to as "graphite" for convenience in the paper). Preserved magmatic quartz is found as colorless or blue porphyroclasts with a rounded and engulfed shape. The frequent habit of quartz and feldspar as broken crystals and shards, attests to explosive dynamics. On the outcrop scale, the color of the metavolcanics is highly variable either over scales of ten centimeters up to several hundred meters, from light gray or pink-gray to black (fig. 3A), with a more or less planar distribution. Evidence that some bleaching by oxidation took place and that the distribution of organic matter was greater than exposed today is the fact that black truncated feldspar porphyroclasts are sometimes disseminated in a light-gray or leucocratic matrix (fig. 3B). In that case, the organic matter was preserved from oxidation only in feldspar porphyroclasts. Thus, light layers may represent zones preserved from carbon introduction or zones in which the carbon was partially oxidized.

Fine-grained tuffs are dark-colored schistose rocks consisting of Qtz + Ab + Phe + Chl and "graphite", in which millimeter-thick or finer quartz-rich layers [microquartzites of possible biogenic origin (Schulz and others, 2001)] evoke a sedimentary layering, tectonically transposed parallel to the foliation. The regular and short wavelength of the layering suggests that these rocks were likely deposited in aquatic, presumably marine, conditions. In some locations (example, Belle-Ile-En-Mer, fig. 2), tuffs predominate over porphyritic volcanics.

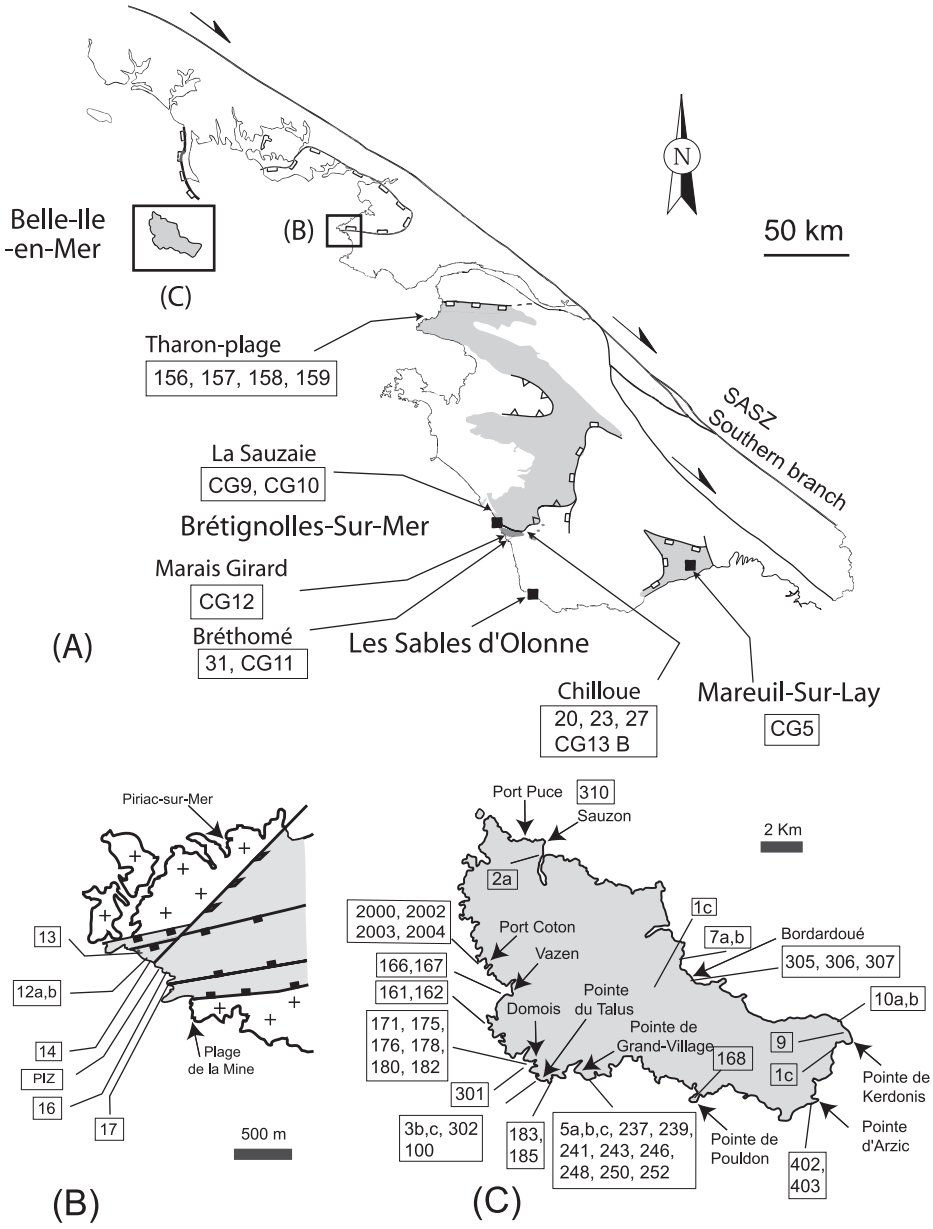


Fig. 2. Location of the samples studied.

At the regional scale, the Porphyroid nappe shows a penetrative flat-lying foliation bearing a strong stretching lineation associated with dominant top-to-the-west shearing (Brun and Burg, 1982; Vauchez and others, 1987). Large strains of up to 400 percent stretching are commonly recorded by truncated feldspar phenocrysts (fig. 3B) (Burg, 1981). From grain-scale to outcrop-scale, deformation features attest to extensive processes of dissolution-crystallization (Vauchez and others, 1987; Le Hébel and

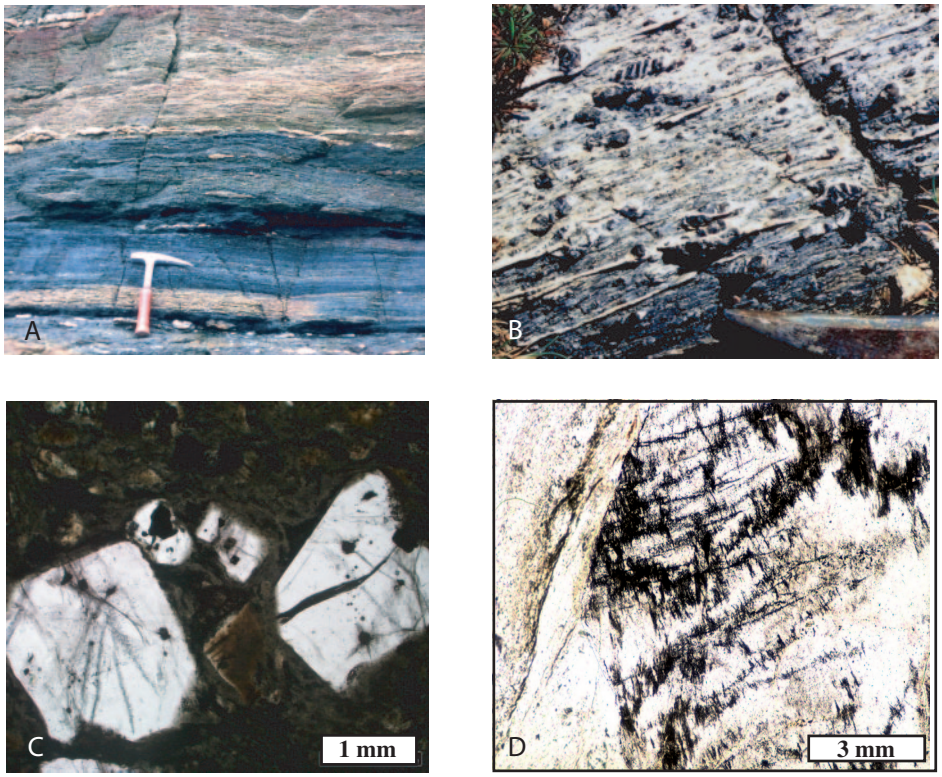


Fig. 3. Outcrop-scale and microscopic-scale aspects of metavolcanics within the Porphyroid nappe (A,B) and within the para-autochthon (C,D). (A) Dark and light layers rich or poor in graphitic compounds, respectively (location: Piriac, fig. 2B); (B) transition between a dark layer (head of the hammer) and a light-gray layer of metavolcanics in the nappe (location: pointe du Talus, Belle-Ile-En-Mer, fig. 2C). The light layer contains truncated black feldspar phenocrysts cemented with white, fibrous quartz, which demonstrates i) that carbon introduction was preceding stretching and ii) that the volumes impregnated with carbon compounds were more widespread than presently observed (see text). (C) Distribution of graphitic matter (ancient oil droplets along annealed cracks) inside a magmatic quartz (undeformed rhyolitic tuff, Chilloue quarry, fig. 2) (XPL); (D) Infiltration of oil (now metamorphosed into graphitic dust) as fischbone-like structures along crystal discontinuities (cleavages and cracks) of an adularitized feldspar porphyroclast (undeformed rhyolitic tuff, Chilloue quarry, fig. 2) (PPL).

others, 2000, 2002a) (figs. 3 and 4). Both quartz and feldspars are involved, leading to the development of a foliation-parallel layering made of alternating quartz-feldspar veins (sinks) and phengite-enriched residual domains (source) (fig. 4D). Dissolution-crystallization occurred under low fluid-rock ratios (Le Hébel and others, 2000, 2002a). Lines of evidence presented by these authors include (i) no break-down of K-feldspar into phengite that behaved as an inert residual phase concentrated within dissolution zones, (ii) mass balance calculations that indicate no volume change at the scale of vein/phengitic selvages systems, (iii) the prevalence of a lithological control on the mineralogical composition of the synkinematic veins (Kfs-bearing veins are localized within Kfs-rich host rocks, and Ab-bearing veins in Kfs-free host rocks), and (iv) sympathetic variations of vein quartz and whole rock O isotopic compositions, attesting to local fluid-vein systems buffered by the host-rock composition.

In the Vendée area, felsic volcanics are also found beneath the basal contact of the Porphyroid nappe (Vauchez and others, 1987 and fig. 1). They are massive, dominantly black porphyritic silicic volcanics (large abundance of graphitic dust in matrix,

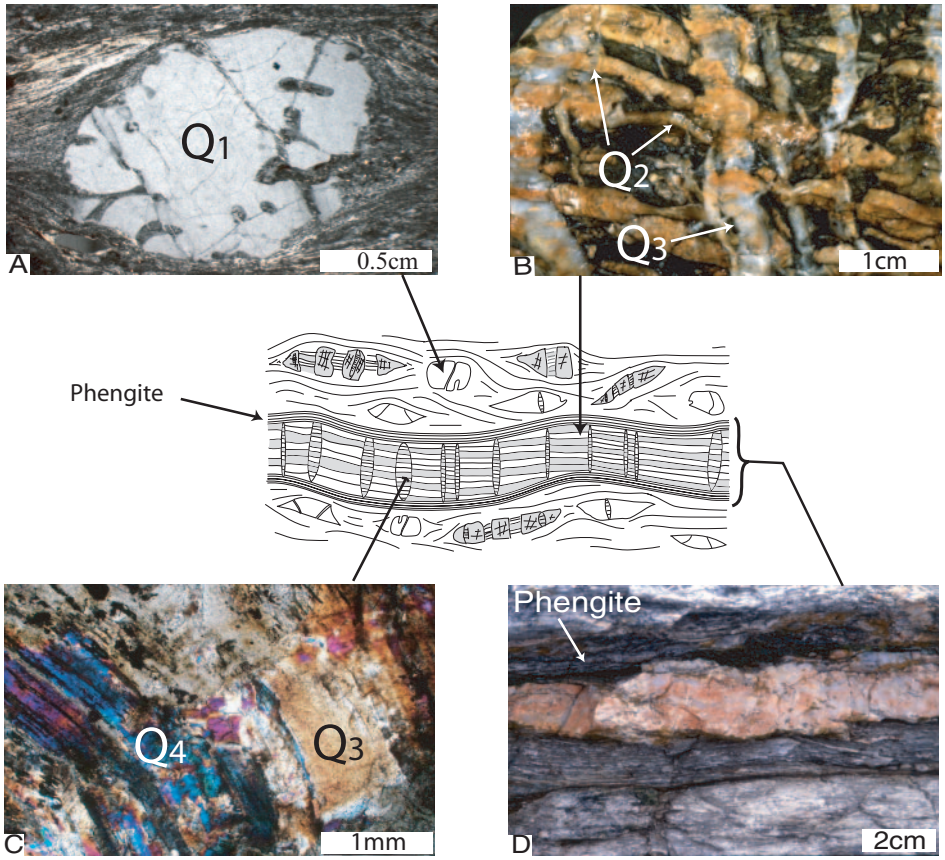


Fig. 4. The four types of successive quartz generations studied ($Q_1$, $Q_2$, $Q_3$, $Q_4$ quartz types discussed in the text) located in a synthetic sketch (center of figure). (A) Volcanic quartz porphyroclast Q1 in thin section (XPL). View is parallel to stretching lineation and perpendicular to foliation. (B) Hand specimen of deformed coarse-grained felsic metavolcanic showing quartz fibers within syn-kinematic quartz-feldspar veins parallel to the foliation (Q2) and within tension gashes affecting these veins (Q3). View parallel to vein surface and foliation. The stretching lineation is sub-equatorial (modified after Le Hébel and others, 2002a). (C) Q3 fibers and Q4 dynamically re-crystallized quartz in thin section (XPL). (D) Field picture showing the phengitic rims bounding a quartz-feldspar vein (modified after Le Hébel and others, 2002a).

feldspars and quartz; figs. 3C and 3D) in which the relative amount of phenocrysts (a few mm in size) is comparable to that of deformed rocks from the nappe. There, the strain intensity decreases downward to undeformed or weakly deformed volcanics over a few tens of meters. These volcanics have the same felsic mineralogy and the same age as those of the overlying nappe. We interpret them as pieces of the low-strain para-autochthonous protolith sliced-off at the base of the main tectonic contact.

Recent U-Pb analyses (SHRIMP) show that the age of the metavolcanics from both the nappe and its para-autochthonous is Lower Ordovician (ca. 480 – 470 Ma; Peucat, unpublished data) and not Upper Silurian-Lower Devonian as was previously proposed on the basis of earlier dating attempts (Talbert and Vialette, 1972; Peucat and others, 1986). The association of the metavolcanics with black shales is a general feature at regional scale. In one locality of the Vendée area, an Upper-Silurian to Lower Devonian age was proposed for the black shales on the basis of microfossil fragments (Peucat and others, 1986). Thus, chronological information shows that the spatial

association of black shales and metavolcanics must be the consequence of thrust tectonics (see sketch of the chronological events in fig. 5).

## SAMPLING STRATEGY

Various analyses were performed on the Porphyroid nappe and on its underlying para-autochthonous counterpart. Sampling sites were selected on the basis of the best rock exposures, the nature of the questions to be solved and the analytical methods used. Sampling areas and sample descriptions are shown in figure 2 and table 1, respectively.

Whole rock compositions (major and trace elements) were investigated for all main sampling localities (Belle-Ile-En-Mer, Piriac, La Sauzaie, and Mareuil-sur-Lay for the nappe; Bréthomé and La Chilloue for the para-autochthon) (fig. 2).

Most of the stable isotope work (present study and Le Hébel and others, 2002a, see table 1) was done on samples from Belle-Ile-En-Mer (fig. 2). In this area, cross-sections of contrasting rock types could be investigated for isotopic variability of whole rocks and individual minerals (see Le Hébel and others, 2000, 2002a and the 1/50 000 map by Audren and Jégouzo, 1986). A few analyses on undeformed rocks were also done on the para-autochthon (Bréthomé, La Chilloue).

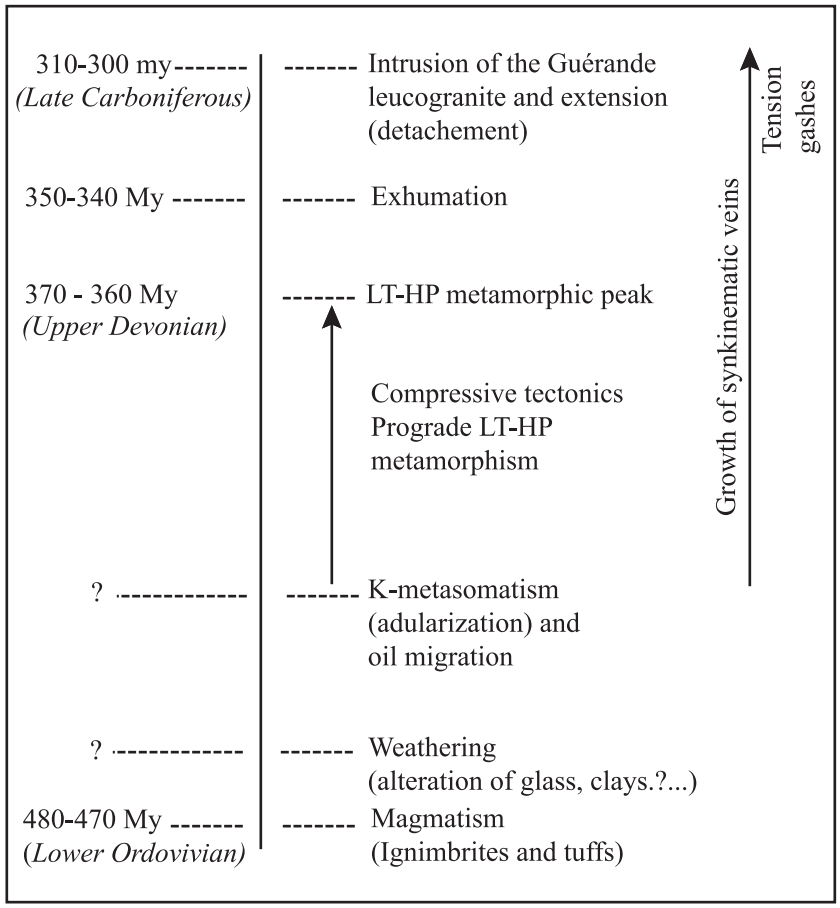


Fig. 5. Sequence of events that affected the metavolcanics from the Porphyroid nappe (see text).

TABLE 1

*Relevant information on the samples studied in the present work (whole-rock O isotopic compositions, C isotopic compositions of graphite, fluid inclusion) and (*) on the samples studied by Le Hébel and others (2002a) (whole-rocks and associated quartz veins, whole-rocks and minerals chemistry).*

| Tectonic Unit | Locality | Sample description | Sample ID | Metamorphic or Alteration minerals | Quartz typology for FI studies |
|---|---|---|---|---|---|
| **Metavolcanics from the Porphyroid nappe** | Belle-Ile-en-Mer (Fig 2C) | ***Coarse-grained porphyritic metavolcanics*** | *, table 2 | Qtz, Adularia, Phe | |
| | | ***Primary magmatic quartz phenocryst*** in coarse-grained porphyritic metavolcanic | * | Qtz | |
| | | ***Synfoliation vein*** in coarse-grained porphyritic metavolcanic | * | Qtz, Adularia | |
| | | ***Late tension gashes*** cutting across the foliation in coarse-grained porphyritic metavolcanic | * | Qtz | |
| | | ***Fine-grained dacitic tuffs*** | table 2 | Qtz, Ab, Chl | |
| | | ***Synfoliation vein*** in fined-grained dacitic tuff | *, table 2 | Qtz, Ab | |
| | | ***Late tension gashes*** cutting across the foliation in fined-grained dacitic tuff | *, table 2 | Qtz | |
| | Piriac-sur-Mer (Fig 2B) | ***Medium-grained porphyritic metavolcanics*** | *, table 2 | Qtz, Adularia, Phe, Ab | |
| | | ***Primary magmatic quartz phenocryst*** in medium-grained porphyritic metavolcanic, displaying intracrystalline deformation and recrystallized quartz neoblasts in shadow zones | FL 14 | Qtz | Clast of volcanic quartz Q1 preserved from recrystallization |
| | | ***Synfoliation vein*** in medium-grained porphyritic metavolcanic | *, table 2 | Qtz + Adul + Phe + Ab | |
| | | ***Late tension gashes*** cutting across the foliation in medium-grained porphyritic metavolcanic | *, table 2 | Qtz | |
| | La Sauzaie (Fig 2A) | ***Coarse-grained porphyritic metavolcanics*** | | Qtz + Adularia + Phe | |
| | | ***Synfoliation vein*** in coarse-grained porphyritic metavolcanic affected by crack-sealing | FL 150 | Qtz + Adularia | Quartz fibers Q2 grown in veins parallel to foliation and quartz fibers Q3 precipitated in cracks |
| | | ***Cracks*** sealed by quartz fibers affected by intracrystalline deformation and dynamic recrystallization (core and mantle structures) | Le Hébel and others (2002a, table 3) | Qtz | Quartz neoblasts Q4 recrystallized at the expense of Q3 fibers |
| **Porphyritic metavolcanics beneath the Porphyroid nappe** | Bréthomé (Fig 2A) | ***Black porphyritic rhyodacitic tuffs*** | FL 145, FL 31 | Qtz, Kfs, Ab rare white micas, Gr | Clast of volcanic quartz Q1 |
| | Chilloue (Fig 2A) | ***Weakly-deformed porphyritic rhyodacitic tuffs*** | table 2 | Qtz, Kfs, Ab, rare white micas, Gr | |
| **Contact zone of the late-kinematic peraluminous Guérande granite** | Métairie Neuve (Fig 2A) | ***Micaschist*** as a roof-pendant within the Guérande granite | MN 1 | Qtz, Bt | Limpid recrystallized quartz in micaschist |
| | | ***Black shale*** as a roof-pendant within the Guérande granite | MN 86-2 | Qtz, Bt, Gr | " " " " |
| | Plage de la Mine (Fig 2A) | ***Cassiterite-bearing quartz vein*** at the contact between Guérande granite and its country-rocks (micaschists) beneath the porphyroid nappe | PNR 1 | Qtz, cassiterite | Milky quartz |

Mineral abbreviations according to Kretz (1983).

Fluid inclusions were studied in all localities, except Belle-Ile-En-Mer, where the fluid inclusions are extremely small-sized and where late kink bands affect the regional foliation and might have disturbed the signature of the main syn-kinematic fluids. To analyze the sequence of fluids, inclusions were studied within a sequence of pre- and syn- kinematic quartz species, as follows.

Pre-metamorphic fluids were investigated from undeformed magmatic quartz beneath the nappe and from relict blue ones within it (Q1, fig. 4A).

Successive syn-kinematic fluids were investigated from the analysis of i) primary quartz fibers elongate parallel to the principal stretch within syn-kinematic veins (Q2, fig. 4B), ii) quartz fibers within secondary tension gashes affecting the syn-kinematic quartz-feldspar veins (Q3, fig. 4C), and iii) quartz neoblasts dynamically recrystallized from syn-kinematic fibers (Q4, fig. 4C).

Fluid inclusions were also studied below the Porphyroid nappe at the roof of the late kinematic Guérande leucogranite emplaced during the latest tectonic stage of Upper Carboniferous extension, around 308 Ma (figs. 1 and 2). Samples are cassiterite-bearing quartz veins cutting granite host-rocks (Plage de la Mine) and recrystallized quartz grains within black shales (Métairie Neuve). The sampling was done to compare fluids released during contact metamorphism of the organic matter in black shales with those from the overlying Porphyroid nappe.

## FLUID INCLUSION AND STABLE ISOTOPE DATA

### *Stable Isotopes*

Oxygen isotopic compositions were measured on whole rocks (WR) and on quartz for different vein generations (table 2; see also data in Le Hébel and others, 2002a). The analytical procedure is described in Appendix 1.

The whole rock $\delta^{18}O$-values of porphyritic material are too high to reflect magmatic values (10.3‰ to 15.1‰; mean = 12.3 ± 1.4‰; table 2) and are secondary compositions, since the highest known $\delta^{18}O$ values for peraluminous magmatism do not exceed 13 permil (example, O'Neil and Chappell, 1977; Fourcade and others, 2001, and references therein). Moreover, in an undeformed sample of the para-autochthon (FL 31, table 2), primary quartz with subhedral shapes has a $\delta^{18}O$ value lower than that of WR (12.4‰ vs. 14.1‰), which indicates a selective $^{18}O$ enrichment of the matrix by isotopic exchange with external fluids at low to moderate temperatures. Fine-grained dacitic tuffs display lower $\delta^{18}O$ values (9 to 12‰, one sample up to 15‰). As a whole, the WR oxygen isotopic compositions are comparable to those recorded in volcanic rocks affected by K-metasomatism with adularization and/or smectite formation (example, Munha and others, 1980; Roddy and others, 1988).

$\delta^{13}C$-values of graphite within both metavolcanics and spatially associated black shales are given in table 3 (analytical procedures in Appendix 1). Graphite from the black shales displays relatively constant $\delta^{13}C$-values around –27.5 permil (vs. PDB), except in the Piriac area where carbon is isotopically heavier ($\delta^{13}C$ = –25.1‰). The $\delta^{13}C$-value of graphitic dust from feldspars or whole rocks in metavolcanics is distinctly lower, ca. –30 permil, except in the Piriac area where it is isotopically heavier (–27.0‰), as observed in the associated black shales (table 3).

### *Fluid Inclusion Characterization*

Analytical techniques are described in Appendix 1.

In all samples, fluid inclusions occur as secondary fluid inclusion planes. Most of them are microcracks (of at most 50 – 100 μm in length) without clear cross-cutting relationships. Usable fluid inclusions along these planes are scarce due to their small

TABLE 2

*O isotopic compositions (WR and one clast of volcanic quartz from non-deformed rhyoignimbrite) of metavolcanics and fine-grained tuffs*

| **Whole-rock sample** *and rock type* | **Locality (Fig. 2)** | **Tectonic unit** | **$\delta^{18}O$ vs. SMOW** | **Error on duplicate** |
|---|---|---|---|---|
| *Coarse-grained metavolcanics* | | | | |
| **FL 2a WR** | *BIEM* | *Porphyroid Nappe* | **13.9** | |
| **FL 3b WR** | *BIEM* | " | **12.1** | **0.2** |
| **FL 3c WR** | *BIEM* | " | **13.34** | **0.01** |
| **FL 5a WR** | *BIEM* | " | **12.0** | |
| **FL 5b WR** | *BIEM* | " | **11.9** | |
| **FL 10b WR** | *BIEM* | " | **15.1** | |
| **FL 176 WR** | *BIEM* | " | **12.72** | **0.02** |
| **FL 178 WR** | *BIEM* | " | **14.5** | **0.1** |
| **FL 180 WR** | *BIEM* | " | **11.6** | |
| **FL 185 WR** | *BIEM* | " | **11.9** | |
| **FL 237 WR** | *BIEM* | " | **11.3** | |
| **FL 239 WR** | *BIEM* | " | **10.6** | |
| **FL 241 WR** | *BIEM* | " | **12.2** | |
| **FL 243 WR** | *BIEM* | " | **11.4** | |
| **FL 250 WR** | *BIEM* | " | **12.6** | |
| **FL 252 WR** | *BIEM* | " | **12.5** | |
| **FL 12a WR** | *Piriac* | " | **10.28** | |
| **FL 12b WR** | *Piriac* | " | **10.58** | |
| **FL 14 WR** | *Piriac* | " | **10.59** | |
| **FL 16 WR** | *Piriac* | " | **10.59** | |
| *Fine-grained (tuffs)* | | | | |
| **FL 171 WR** | *BIEM* | *Porphyroid Nappe* | **10.3** | |
| **FL 175 WR** | *BIEM* | " | **10.3** | |
| **FL 182 WR** | *BIEM* | " | **9.0** | |
| **FL 183 WR** | *BIEM* | " | **9.7** | |
| **FL 246 WR** | *BIEM* | " | **9.9** | |
| **FL 248 WR** | *BIEM* | " | **15.0** | |
| *Coarse-grained metavolcanics* | | | | |
| **FL 20 WR** | *Chilloue* | *Parautochton* | **13.84** | |
| **FL 23 WR** | *Chilloue* | " | **14.34** | |
| **FL 27 WR** | *Chilloue* | " | **10.93** | |
| **FL 31 WR (+ Qtz)** | *Bréthomé* | " | **14.14 (Qtz =12.38)** | **(0.02)** |

Other quartz and WR O isotopic compositions discussed can be found in Le Hébel and others (2002a). Sampling localities (fig. 2) include Belle-Ile-En-Mer (BIEM) and Piriac-Sur-Mer within the Porphyroid nappe, and Bréthomé and Chilloue in the para-autochthon beneath the nappe.

TABLE 3

*Carbon isotopic composition of graphitic matter*

| **Sample** (Fig. 2) | **"graphite"** *in* | **Tectonic unit** | **locality** | $\delta\ ^{13}C$ vs. PDB | **deviation** |
|---|---|---|---|---|---|
| **FL 301** | black schist | *Porphyroid nappe* | *BIEM (Domois-Le Talus)* | - 27.55 | 0.04 |
| **FL 302** | black feldspar | " | *BIEM (Le Talus)* | - 29.80 | 0.07 |
| **FL 3b** | black meta-volcanic | " | *BIEM (Le Talus)* | - 30.15 | 0.08 |
| **FL 305** | black schist | " | *BIEM (Bordardoué # 3)* | - 27.31 | |
| **FL 306** | black schist | " | *BIEM (Bordardoué # 4)* | - 27.14 | |
| **FL 307** | black schist | " | *BIEM (Bordardoué # 5)* | - 27.51 | |
| **PiZ** | black schist | " | *Piriac* | - 25.07 | |
| **FL 17** | Black meta-volcanic | " | *Piriac* | - 26.99 | 0.08 |
| **FL 31** | black rhyolite | *Parautochton* | *Chilloue* | - 28.85 | |
| **CG 13 b** | black rhyolite | " | *Bréthomé* | - 30.13 | 0.01 |
| **USGS 24** | | | | -15.97 | 0.06 (113) |

See text for comments.

BIEM: Belle-Ile-En-Mer (in the Bordardoué locality, the number given indicates which of the 7 black shale layers outcropping from E to W were analyzed).

Deviation indicated corresponds to duplicates.

size, and time-relationships are therefore rather difficult to establish. However, within a given plane, the density of fluid inclusions is rather constant. This indicates that the studied planes contain well-preserved inclusions corresponding to a given stage of the fluid history.

The nomenclature of fluid inclusions follows the convention of Boiron and others (1992). It is based on the type of total homogenization Th (L-V to the vapor noted V, L-V to the liquid noted L) and the nature of the fluid component (subscript c, m, n or w for $CO_2$, $CH_4$, $N_2$ and $H_2O$ respectively), as a function of the abundance of the various species in the fluid. Table 4 specifies the meaning of the used abbreviations. Three main fluid types are distinguished on the basis of their morphologies, microthermometric properties, and on the different species present in the inclusions. They have a variety of densities which results in a series of inclusions homogenizing either in the liquid or the vapor phase:

— aqueous-carbonic (noted c-w) inclusions with significant amounts of $CO_2$ (Lc-w, Vc-w),

— aqueous-carbonic inclusions with minor amounts of volatiles (Lw-c, Vw-c),

— inclusions dominated by $CO_2$ (Lc, Vc) or by methane with some amounts of nitrogen (Vm-n), where the water content is low and any quantitative optical estimate difficult, especially in small inclusions.

Fluid inclusions representative of the three main types of fluid have been analyzed by microthermometry and Raman spectroscopy to determine their density and composition (tables 5 and 6).

*Preserved magmatic quartz below the nappe (Bréthomé).*—In the non-deformed black-colored volcanics, quartz clasts display different types of inclusions (fig. 6).

Table 4

*Typology and nomenclature of fluid inclusions*

| Type of fluid inclusions | Dominant species | Observations |
|---|---|---|
| Lc-w or Vc-w | $CO_2$-($CH_4$-$N_2$)-$H_2O$-NaCl | Tm $CO_2$ and Th $CO_2$ observed<br>$CH_4$+ $N_2$< 10 mol.% in the volatile phase |
| Lw-c or Vw-c | $H_2O$-$CO_2$-($CH_4$-$N_2$)- NaCl | Only Tm cl observed<br>Low density volatile phase<br>$CH_4$+ $N_2$< 30 mol.% in the volatile phase |
| Lc or Vc | $CO_2$-$CH_4$-$N_2$ | Tm $CO_2$ and Th $CO_2$ observed<br>$CH_4$+ $N_2$< 30 mol.% in the volatile phase<br>No visible water |
| Vm-n | $CH_4$-$N_2$ | Only Th $CH_4$ observed<br>No visible water |

Tm $CO_2$, Tm cl, Tm ice: melting temperature of $CO_2$, clathrate and ice, respectively. Th $CO_2$, Th $CH_4$: homogenization temperature of $CO_2$ and of $CH_4$, respectively. Td: decrepitation temperature. All values are in °C. L or V subscripts mean a total homogenization to the liquid phase (L) or to the vapor phase (V).

Most fluid inclusions display regular shapes, are black-colored, with sizes ranging from 5 to 10 μm (fig. 6A). They occur as sub-horizontal planes. These Lc-w inclusions contain two fluid phases at room temperature with degree of volatile fillings > 80 to 90 percent. Melting temperature of $CO_2$ (Tm $CO_2$) is in the range –57.9 to –57.8°C and homogenization temperature of $CO_2$ (Th $CO_2$) to the liquid phase in the range +7.9 to +13.7°C. Hydrocarbons detected in these inclusions by Raman spectroscopy prevents gas quantification ($CO_2$-$CH_4$-$N_2$).

Vc-w inclusions also display regular shapes. They contain three fluid phases at room temperature with volatile fillings of 40 to 50 percent. They show Tm $CO_2$ in the range of –58.6 to –58.9°C, significantly lower than the melting temperature of pure $CO_2$, which indicates the presence of volatile compounds other than $CO_2$, such as $CH_4$ and $N_2$. Th $CO_2$ occurs to the vapor phase in the range +14.1 to +17.1°C. Melting temperature of clathrate (Tm cl) ranges from +3.2 to +6.7°C, melting temperature of ice (Tm ice) from –4.3 to –6.2°C, and homogenization temperature (Th) (to the vapor phase) from +371 to +392°C. Hydrocarbons have been detected by Raman spectroscopy in some of these Vc-w inclusions.

*Inherited magmatic quartz clasts from the deformed units (Porphyroid nappe, Piriac-sur-Mer).*—Different types of fluid inclusions have been distinguished according to their morphology.

— Annular and semi-annular inclusions were mostly observed as isolated inclusions (fig. 6B). This typical atoll-like shape is attributed to a short-lived increase of the confining pressure under a non-isotropic stress field (Boullier and others, 1991; Tecce and others, 2001) and could be associated with re-equilibration of inclusions during isothermal decompression.

— Black decrepitated inclusions display dendritic contours and "star" shapes and are surrounded by small inclusions (fig. 6C). Raman analyses performed on these inclusions, modified after trapping, indicate the presence of graphite and $CO_2$+$CH_4$ gases.

— Preserved aqueous-carbonic inclusions are characterized by regular shapes and constitute the only "unmodified" fluid relicts (fig. 6D). They may contain one unidentified solid (white and limpid). At room temperature, Lc-w inclusions are three-phase (liquid $H_2O$, liquid $CO_2$ and gaseous $CO_2$), with a degree

TABLE 5

*Summary of microthermometric data obtained on the different types of fluid inclusions*

| Quartz type | Inclusion type | Inclusion morphology | Size | Degree of volatile filling | Microthermometry (°C) Tm $CO_2$ | Th $CO_2$ | Tm cl | Tm ice | Th |
|---|---|---|---|---|---|---|---|---|---|
| **Clast of volcanic quartz (Q1) in non-deformed metavolcanics beneath the nappe (Bréthomé, Bas Bocage)** | **Lc-w** | FIP regular rounded shapes | 5-10 µm | 80-90% | -57.9/-57.8 | 7.9/13.7 L | nv | nv | nv |
| | **Vc-w** | unidentified solid | 7-15 µm | 40-50% | -58.9/-58.6 | 14.1/17.1 V | 3.2/6.7 | -6.2/-4.3 | 371/392 V |
| **Clast of volcanic quartz (Q1) in deformed metavolcanics from the nappe (Piriac-sur-Mer)** | **Lc-w** | regular shapes observed as more or less continuous FIP | 5- 8 µm | 10-20% | -61.3/-59.0 | 15.6/23.4 L or V | 2.5/8.1 | -4.2/-0.2 | 323/415 L or V |
| **Quartz veins parallel to foliation (La Sauzaie-Vendée)** | **Lc-w** | FIP irregular shape | 5-10 µm | 20-30% | -59.2/-57.6 | 6.1/26.2 L or V | 6.5/8.1 | nv | 248 L or Td<272 |
| **Fibrous veins (Q2 and Q3)** | **Vw-c** | parallel to the stretching lineation | 5-10 µm | 60% | -57.9 | nv | 7.9 | -4.5 | Td<272 |
| | **Lw-c** | | 5-10 µm | 20-30% | nv | nv | 5.1 | -5.5 | Td<272 |
| **Recrystallized quartz neoblast (Q4) (La Sauzaie-Vendée)** | **Lc-w** | FIP regular rounded shape | 5-10 µm | 20-30% | -59.0/-57.4 | 19.5/28.0 L or V | 7.6/9.0 | -7.5/-7.0 | nv |
| | **Vc-w** | | 7-15 µm | 50-60% | -58.9/-58.6 | 20.9 V | 8.1/8.7 | nv | nv |
| | **Lw-c** | | 7-15 µm | 20-30% | nv | nv | 9.6 | -5.7 | nv |
| | **Lc** | | 10 µm | 100% | -59.7 | 9.2/10.8 L | nv | nv | nv |
| **Recrystallized quartz in black schists (Métairie Neuve)** | **Vm-n** | FIP regular shape | 10-15 µm | 100% | | -96.4/-88.3 V (Th $CH_4$) | nv | nv | nv |
| **Cassiterite-bearing quartz vein (Plage de la Mine)** | **Lw-c** | regular rounded shapes observed as more or less continuous FIP | 20 µm | 40% | -59.8/-59.4 | nv | 9.1/11.6 | -5.1/-6.9 | 343 L or Td<343 |
| | **Lc - Vc** | | 10-15 µm | 100% | -60.7 /-61.3 | -3.3/-0.7 L or V | nv | nv | nv |

Abbreviations are the same as in table 4. nv: not visible, FIP: Fluid Inclusion Plane. Q1, Q2, Q3, Q4 quartz types are defined in text and figure 4.

of volatile filling around 10 to 20 percent. Tm $CO_2$ ranges from –59.0 to –61.3°C. Th $CO_2$ occurs to the liquid phase in the range +15.6 to +17.5°C or, to the vapor phase, at around +23.4°C. Tm cl is ranging from +2.5 to +8.1°C. Tm ice ranges between –0.2 and –4.2°C. Some fluid inclusions decrepitated before homogenization at temperatures up to +323°C; the few measured Th range from +323 to +415°C.

*Quartz fibers in the Porphyroid nappe (La Sauzaie).*—In fibrous quartz, most inclusions are distributed in sub-vertical planes parallel to fibers underlying the stretching lineation (fig. 6E). These planes mainly display black decrepitated inclusions displaying dendritic contours and no fluid remnant. However, a few fluid inclusions are preserved in some planes. Among them, three main types have been distinguished.

— Aqueous-carbonic (Lc-w) inclusions with irregular shapes, sizes ranging from 5 to 10 μm, and generally elongate parallel to the stretching direction. At room temperature, these inclusions contain liquid $H_2O$, liquid $CO_2$ and gaseous $CO_2$, with a homogenous degree of volatile filling, around 20 to 30 percent. Tm $CO_2$ ranges from –59.2 and –57.6°C. Th $CO_2$ occurs in the liquid or vapor phase in the range +6.1 to +26.2°C. Tm cl is between +6.5 to +8.8°C.

— Vw-c inclusions contain two fluid phases at room temperature, with a degree of volatile filling around 60 percent. Tm $CO_2$ and Tm cl are measured at –57.9°C and around +7.9°C, respectively. Tm ice is around –4.5°C.

— Lw-c inclusions display irregular shapes and are generally elongate parallel to the stretching direction. At room temperature, they contain two fluid phases (liquid $CO_2$ - liquid $H_2O$) with a constant degree of volatile filling around 20 to 30 percent. Only Tm cl and Tm ice have been measured, around +5.1°C and –5.5°C, respectively.

Most of these three types of inclusions decrepitated before homogenization at temperatures up to +270°C.

*Dynamically re-crystallized neoblasts from quartz fibers (La Sauzaie).*— In neoblasts, fluid inclusions are distributed in non-oriented planes. Four main types have been distinguished.

— Lc-w inclusions displaying regular rounded shape are three-phase (liquid $H_2O$, liquid $CO_2$ and gaseous $CO_2$,) inclusions at room temperature, with a homogenous degree of volatile filling around 20 to 30 percent. Tm $CO_2$ ranges from –59.0 and –57.4°C and Th $CO_2$ (to the liquid or vapor phase) from +19.5 to +28.0°C. Tm cl and Tm ice range from +7.6 to +9.0°C and from –7.5 to –7.0°C, respectively. Rare single-phase Lc inclusions have been observed. Tm $CO_2$ is measured at –59.7°C and Th $CO_2$ occurs to the liquid phase in the range +9.2 to +10.8°C.

— Vc-w inclusions contain three fluid phases at room temperature, with a homogeneous degree of volatile filling around 50 to 60 percent. Tm $CO_2$ was measured between –58.9 and –58.6°C, Th $CO_2$ (to the vapor phase) around +20.9°C and Tm cl in the range +8.1 to +8.7°C.

— Lw-c inclusions contain two fluid phases (liquid $CO_2$ - liquid $H_2O$) at room temperature, with a constant degree of volatile filling around 20 to 30 percent. Only Tm cl and Tm ice have been measured, around +9.6°C and –5.7°C, respectively.

Most inclusions decrepitated before homogenization.

*Contact zones with the Guérande peraluminous granite.*—a) Re-crystallized quartz grains in black shales (Métairie Neuve). Fluid inclusions are single-phase at room temperature and they display rounded shapes (10 to 15 μm) along inclusion planes (figs. 6F and 6G). After cooling to –180°C, they become two-phase inclusions which homogenize to the vapor phase in the range –88.3 to –96.4°C. Such Vm-n fluid

TABLE 6

*Chemical composition of typical fluid inclusions from the different studied areas obtained by Raman spectroscopy and corresponding microthermometric data*

| Quartz type (Fig. 2) | FI type | Microthermometry (°C) | | | | | Raman data (mol.%) | | | | Bulk composition (mol. %) | | | | |
|---|---|---|---|---|---|---|---|---|---|---|---|---|---|---|---|
| | | Tm $CO_2$ | Th $CO_2$ | Tm cl | Tm ice | Th | $CO_2$ | $CH_4$ | $N_2$ | $H_2S$ | $H_2O$ | $CO_2$ | $CH_4$ | $N_2$ | NaCl |
| **Clast of volcanic quartz (Q1) in non-deformed metavolcanics beneath the nappe (Bréthomé, Bas Bocage)** | Vc-w | -58.6 | 17.1 V | 4.0 | -6.2 | 392 V | 94.3 | HC | 5.7 | nd | 88.6 | 7.6 | - | 0.3 | 3.5 |
| | Vc-w | -58.9 | 14.1 V | 6.7 | -4.3 | 371 V | 100 | HC | 0 | nd | 91.0 | 7.0 | - | - | 2.0 |
| | Vc-w | -58.8 | 14.8 V | 3.2 | -4.7 | 380 V | 89.3 | 1.5 | 9.2 | nd | 85.7 | 9.6 | 0.1 | 0.7 | 3.9 |
| **Clast of volcanic quartz (Q1) in deformed metavolcanics from the nappe (Piriac-sur-Mer)** | Lc-w | -59.1 | nv | nv | -0.5 | 323 L | 95.6 | 0.7 | 3.7 | nd | 98.1 | 1.9 | tr | tr | - |
| | Lc-w | -59.4 | nv | nv | nv | nv | 93.6 | 3.4 | 3.0 | nd | 97.0 | 3.0 | tr | tr | - |
| | Lc-w | -59.3 | nv | nv | -0.2 | 370 L | 97.8 | 0.6 | 1.6 | nd | 97.8 | 2.2 | tr | tr | - |
| | Lc-w | -59.0 | 23.4 V | 3.0 | -4.2 | 415 L | 97.3 | 0.7 | 2.0 | nd | 87.2 | 8.6 | 0.1 | 0.1 | 4.0 |
| | Lc-w | -59.1 | 17.5 L | 3.4 | -0.3 | <323 D | 96.0 | 0.7 | 3.3 | nd | 85.7 | 10.0 | 0.05 | 0.3 | 3.95 |
| | Lc-w | -59.8 | 15.6 L | 8.1 | nv | <323 D | 93.5 | 4.3 | 2.2 | nd | 91.8 | 5.9 | 0.2 | 0.1 | 2.0 |
| | Lc-w | -59.1 | 17 L | 3.2 | -0.2 | nv | 96.3 | 1.2 | 2.5 | nd | 87.7 | 7.9 | 0.1 | 0.1 | 4.2 |
| | Lc-w | -61.3 | 16.7 L | 2.6 | -0.2 | nv | 93.0 | 3.7 | 3.3 | nd | 89.4 | 5.6 | 0.2 | 0.1 | 4.7 |
| **Quartz fibers (Q2) within syn-kinematic quartz veins parallel to foliation (La Sauzaie-Vendée)** | Lc-w | -57.6 | nv | 7.5 | -5.5 | 272 D | 93.1 | 4.3 | 2.6 | nd | 93.6 | 4.7 | 0.1 | 0.05 | 1.55 |
| | Lc-w | -59.0 | 26.2 L | 8.1 | nv | 272 D | 95.3 | 1.7 | 3.0 | nd | 88.2 | 10.2 | 0.1 | 0.2 | 1.3 |
| | Lc-w | -58.8 | 9.8 L | 7.2 | nv | 272 D | 93.1 | 5.2 | 1.7 | nd | 91.0 | 6.0 | 0.2 | 0.1 | 2.7 |
| **Quartz from fibrous veins (Q3) within tension gashes (La Sauzaie, Vendée)** | Lc-w | -58.7 | 6.1 L | 6.5 | nv | 272 D | 91.2 | 6.0 | 2.8 | nd | 81 | 14.3 | 0.8 | 0.4 | 3.5 |
| | Lc-w | -59.2 | 23.1 V | 7.9 | nv | 248 L | 94.3 | 3.6 | 2.1 | nd | 93.1 | 5.2 | 0.1 | 0.1 | 1.5 |
| | Lc-w | -58.2 | 21.5 V | 7.4 | nv | 272 D | 93.4 | 2.2 | 4.4 | nd | 91.8 | 6.1 | 0.1 | 0.2 | 1.8 |
| | Lw-c | nv | nv | 5.1 | -5.5 | <272 D | 93.3 | 4.3 | 2.4 | nd | 94.5 | 3.6 | 0.05 | 0.05 | 1.8 |
| | Vw-c | -57.9 | nv | 7.9 | -4.5 | 272 D | 94.3 | 1.8 | 3.9 | nd | 92 | 6.8 | 0.1 | 0.2 | 0.9 |

Q1, Q2, Q3, Q4 quartz types are defined in text and figure 4. Compositions are given in mol. %. Abbreviations are the same as in tables 4 and 5. tr: traces, D: decrepitation. *: For Lc and Vc inclusions, bulk composition has been calculated assuming a 10% maximum degree of liquid filling.

TABLE 6
*(continued)*

| Quartz type (Fig. 2) | FI type | Microthermometry (°C) | | | | | Raman data (mol.%) | | | | Bulk composition (mol. %) | | | | |
|---|---|---|---|---|---|---|---|---|---|---|---|---|---|---|---|
| | | Tm $CO_2$ | Th $CO_2$ | Tm cl | Tm ice | Th | $CO_2$ | $CH_4$ | $N_2$ | $H_2S$ | $H_2O$ | $CO_2$ | $CH_4$ | $N_2$ | NaCl |
| **Recrystallized quartz neoblast (Q4) (La Sauzaie-Vendée)** | **Lc-w** | -58.6 | 22.7 L | 7.8 | nv | nv | 92.2 | 2.3 | 5.5 | nd | 86.4 | 11.5 | 0.2 | 0.5 | 1.4 |
| | **Lc-w** | -57.6 | 23.2 L | 8.2 | nv | nv | 92.7 | 2.5 | 4.8 | nd | 86.8 | 11.5 | 0.2 | 0.5 | 1.0 |
| | **Lc-w** | -59.0 | 19.5 L | 9.0 | nv | nv | 90.2 | 4.1 | 5.7 | nd | 91.3 | 7.6 | 0.2 | 0.3 | 0.6 |
| | **Lc-w** | -57.4 | 20.9 L | 8.7 | nv | nv | 90.0 | 4.4 | 5.6 | nd | 87.7 | 10.6 | 0.4 | 0.5 | 0.8 |
| | **Lc-w** | -58.3 | 24.3 V | 8.8 | -7.0 | nv | 94.3 | 1.6 | 4.1 | nd | 93.2 | 5.7 | 0.05 | 0.1 | 0.95 |
| | **Lc-w** | -57.8 | 28 V | 7.6 | -7.5 | nv | 93.5 | gr | 6.5 | nd | 90.2 | 7.8 | - | 0.4 | 1.6 |
| | **Vc-w** | -58.6 | 20.9 V | 8.1 | nv | nv | 88.3 | 2.9 | 8.8 | nd | 83.7 | 13.8 | 0.4 | 1.1 | 1.0 |
| | **Vc-w** | -58.9 | 20.9 V | 8.7 | nv | nv | 89.7 | 4.8 | 5.5 | nd | 88.9 | 9.5 | 0.4 | 0.4 | 0.8 |
| | **Lw-c** | nv | nv | 9.6 | -5.7 | nv | 79.3 | 4.4 | 16.3 | nd | 93.3 | 4.6 | 0.1 | 0.5 | 1.5 |
| | **Lc*** | -59.7 | 10.8 L | | | | 84.0 | 2.6 | 13.4 | nd | 26.1 | 62.2 | 1.9 | 9.8 | - |
| | **Lc*** | -59.7 | 9.2 L | | | | 86.1 | 3.0 | 10.9 | nd | 25.2 | 64.5 | 2.2 | 8.1 | - |
| | | | **Th $CH_4$** | | | | | | | | | | | | |
| **Recrystallized quartz in black schists (Métairie Neuve)** | **Vm-n** | | -95.5 V | | | | nd | 85.1 | 14.2 | nd | | | | | |
| | **Vm-n** | | -95.5 V | | | | nd | 85.2 | 14.8 | nd | | | | | |
| | **Vm-n** | | -96.4 V | | | | nd | 87.2 | 12.8 | nd | | | | | |
| | **Vm-n** | | -88.3 V | | | | nd | 86.4 | 13.6 | nd | | | | | |
| | **Vm-n** | | -89.3 V | | | | nd | 86.4 | 13.6 | nd | | | | | |
| **Cassiterite-bearing quartz vein (Plage de la Mine)** | **Lw-c** | -58.9 | nv | 10.1 | nv | <343 D | 73.7 | 10.8 | 15.0 | 0.5 | 90.7 | 6.8 | 0.7 | 0.9 | 0.9 |
| | **Lw-c** | -59.4 | nv | 11.6 | -5.1 | <343 D | 67.5 | 16.5 | 15.5 | 0.5 | 86.9 | 9.4 | 1.8 | 1.7 | 0.2 |
| | **Lw-c** | nv | nv | 9.1 | -3.9 | 343 L | 65.5 | 17.0 | 17.0 | 0.5 | 93.1 | 4.6 | 0.6 | 0.6 | 1.1 |
| | **Vc*** | -60.7 | -2 V | | | | 69.2 | 13.3 | 17.0 | 0.5 | 64.4 | 26.6 | 3.8 | 5.2 | - |
| | **Lc*** | -61.2 | -3.3 L | | | | 75.0 | 10.5 | 14.0 | 0.5 | 28.1 | 54.6 | 7.4 | 9.9 | - |
| | **Lc*** | -61.3 | -0.7 L | | | | 73.0 | 11.5 | 15.0 | 0.5 | 26.5 | 54.4 | 8.3 | 10.8 | - |

Q1, Q2, Q3, Q4 quartz types are defined in text and figure 4. Compositions are given in mol. %. Abbreviations are the same as in tables 4 and 5. tr: traces, D: decrepitation. *: For Lc and Vc inclusions, bulk composition has been calculated assuming a 10% maximum degree of liquid filling.

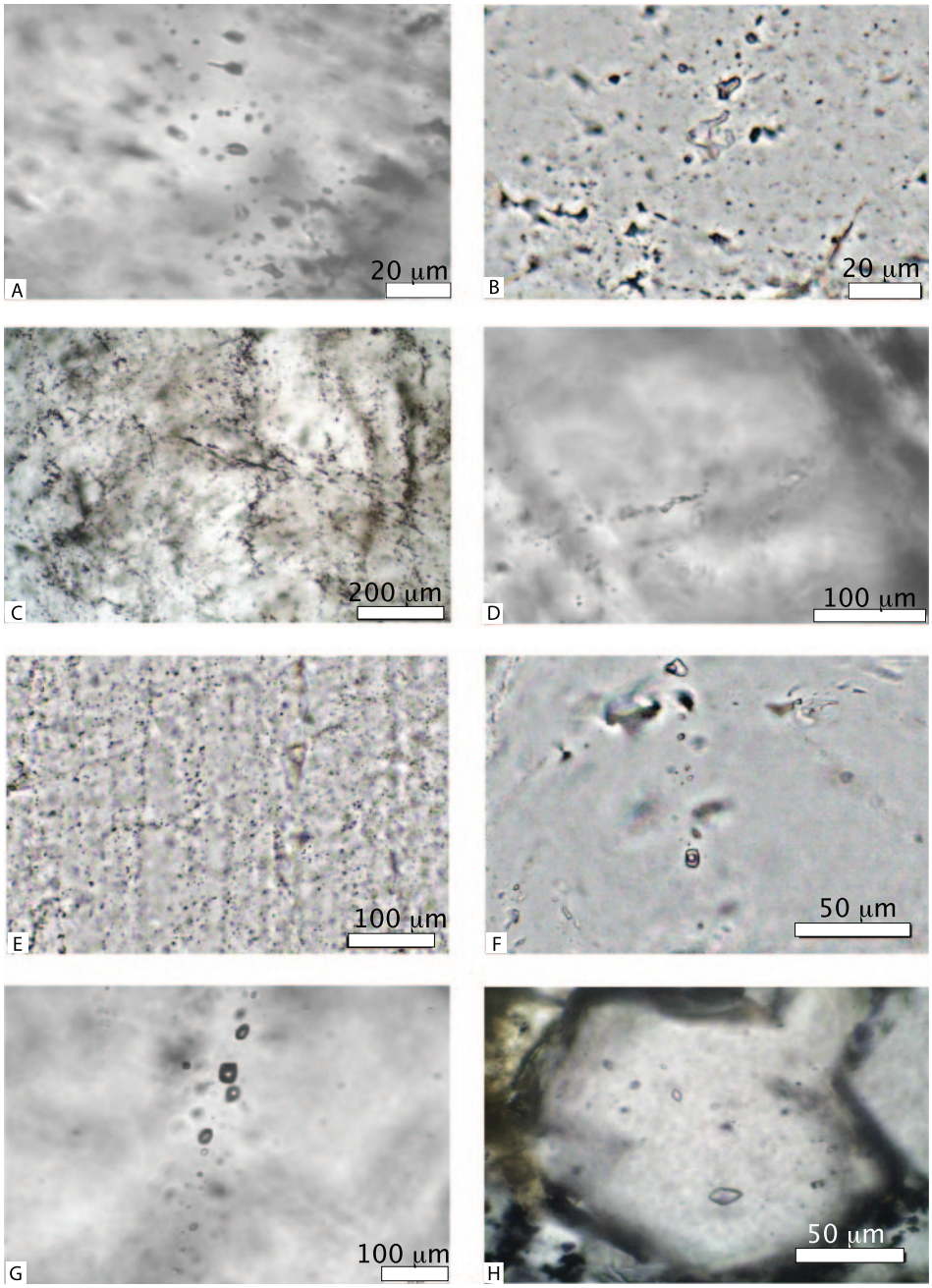


Fig. 6. Typical fluid inclusion morphologies found in the studied quartz samples (PPL). (A) Aqueous-carbonic Lc-w inclusions in quartz from the Porphyritic lavas beneath the nappe (Bréthomé). (B) Annular inclusion in inherited magmatic quartz clasts from the deformed units (Porphyroid nappe, Piriac-sur-Mer). (C) Black decrepitated inclusions in inherited magmatic quartz clasts from the deformed units (Porphyroid nappe, Piriac-sur-Mer). (D) Preserved Lc-w inclusions in inherited volcanic quartz clasts from the deformed units (Porphyroid nappe, Piriac-sur-Mer). (E) Fluid inclusion planes in quartz veins parallel to the foliation in deformed metavolcanics from the Porphyroid nappe (La Sauzaie). (F) and (G) $CH_4$-$N_2$ rich inclusions in clear quartz from contact-metamorphosed black shales (Métairie Neuve). (H) Aqueous-carbonic inclusions in quartz -(cassiterite) dike (Plage de la Mine).

inclusions are dominated by $CH_4$ with some amounts of $N_2$. $CO_2$ was not detected by Raman spectroscopy. b) Quartz veins (Plage de la Mine). In quartz veins in the granite roof, most fluid inclusions display rounded and regular shapes and are observed as more or less continuous fluid inclusion planes.

Lw-c inclusions (fig. 6H) contain two fluid phases at room temperature, with a degree of volatile filling around 40 percent. Tm $CO_2$ ranges from –59.4 to –59.8°C, Tm cl from +9.1 to +11.6°C and Tm ice from –3.3 to –6.9°C. One Th (to the liquid phase) has been measured at +343°C.

Lc and Vc inclusions are single-phase at room temperature. They show Tm $CO_2$ in the range –60.7 to –61.3°C and Th $CO_2$ from –3.3 to –0.7° C.

*Composition of Volatile Phase, Density and Bulk Chemical Evolution of Major Components*

Analytical techniques are described in Appendix 1.

*Volatile phase composition and density.*—As a whole, the studied fluids typically belong to the C-H-O-N system, with a volatile phase dominated by $CO_2$ (>88 mol. %). $CH_4$ and $N_2$ are present and contents range from 0.5 to 6 mole percent and from 0 to 9 mole percent, respectively. Locally, some fluid inclusions show an enrichment in $N_2$ up to 16 mole percent (table 6 and fig. 7). Fluid inclusions observed in recrystallized quartz in black shales from Métairie Neuve are dominated by $CH_4$ (around 85 mol.%) and $N_2$ (12 to 15 mol. %).

The relative amount of $CO_2$ in the volatile phase as a function of the non-aqueous volatile density shows a strong variation of the volatile phase density from a maximum of 0.80 g/cm$^3$ for the three-phase inclusions down to a minimum of 0.1 g/cm$^3$ at nearly constant composition (fig. 8). This decrease is observed in most of the representative inclusions analyzed in deformed metavolcanics from the Porphyroid nappe (quartz veins and quartz volcanic clasts). It indicates that fluid inclusions have likely recorded strong variations of pressure, with no important changes in the fluid composition during exhumation. In contrast, only low-density fluid inclusions (Vc-w densi-

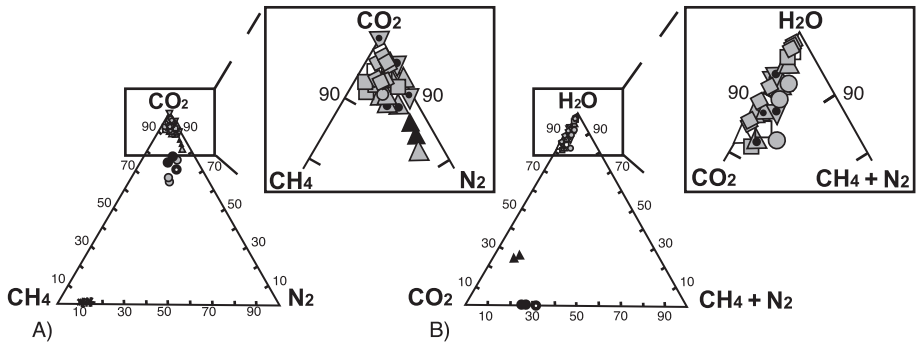


Fig. 7. Geochemistry of the aqueous-carbonic fluids from the different studied areas. (A) $CO_2$-$CH_4$-$N_2$ ternary plot (compositions of the volatile phase obtained by Raman analysis), (B) $H_2O$-$CO_2$-$CH_4$+$N_2$ ternary plot (calculated bulk fluid composition), with enlargement of the zone of interest. Abbreviations for the different types of fluids are defined in table 4 and in the text.

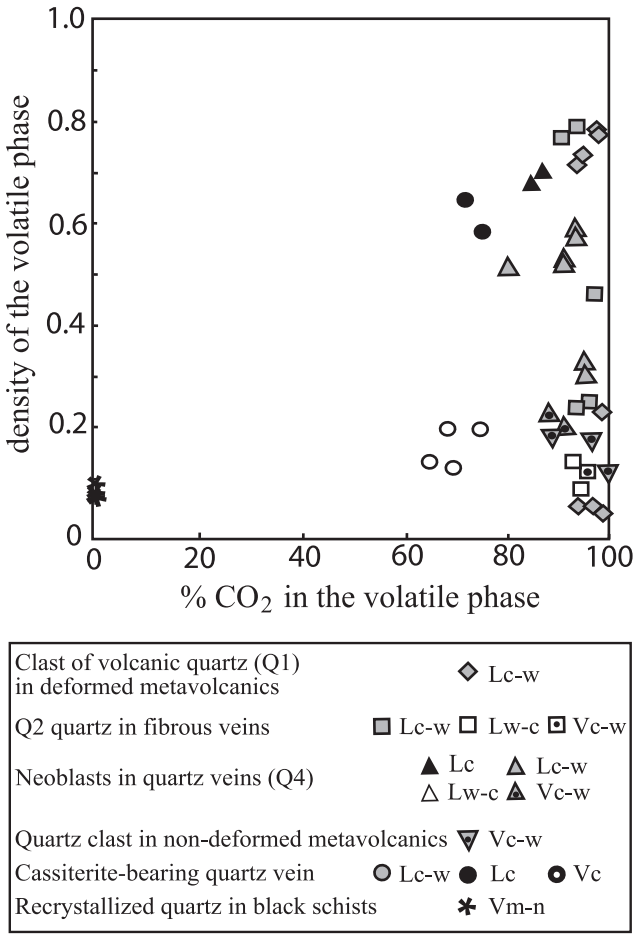


Fig. 8. Density versus $CO_2$ content (in mol.%) of the volatile phase for the aqueous-carbonic fluids from the different studied areas.

ties, ranging from 0.12 to 0.19 g/cm$^3$) have been found in the non-deformed porphyritic lavas beneath the nappe. The $CH_4$-$N_2$ fluids are vapors that also have low densities.

*Bulk composition.*—The aqueous-carbonic fluids are water-dominated (>84 mol.%) with variable amounts of $CO_2$ (2 to 15 mol. %), and small amounts of $CH_4$ (<0.8 mol. %) and $N_2$ (<1.1 mol.%) (fig. 7). Salinity (given in mol. % eq NaCl) ranges from 0.6 to 4 mole percent. Such compositions are typical of fluids equilibrated with metamorphic host-rocks that have experienced pressure variations (Huizenga, 2001).

In the few (small-sized) inclusions dominated by $CO_2$ (Lc, Vc) or by $CH_4$ (Vm-n), water is not visible optically. Nevertheless, the water content may reach 10 percent in such inclusions considering the spatial resolution of a good microscope (Dubessy and others, 1992). This maximum estimate of the water content corresponds to 25 to 30 mole percent in the bulk composition (table 6). The single-phase $CH_4$-rich inclusions mentioned above were observed in most metamorphosed black schists from the Paleozoic of western Europe. They are interpreted as the result of devolatilization of these lithologies in the presence of very low amounts of water (Boiron and others,

2003). The $CO_2$-rich inclusions from the cassiterite quartz veins may result from intermittent immiscibility.

## DISCUSSION

### *Early Diagenetic Evolution. Metasomatic Alteration and Oil Migration*

Even though the petrography of the studied rocks argues for a volcanic origin, their chemical compositions, in particular high K/Na ratios (fig. 9) document intense metasomatic alteration. Rock identification, protolith characteristics and geodynamic setting based on elements assumed to be immobile during alteration and on radiogenic isotopes will be presented in another paper. Summarizing the available data (Le Hébel, ms, 2002), the rocks studied pertain to calc-alkaline series, the felsic porphyritic rocks have rhyolitic to rhyodacitic compositions, the fine-grained tuffs have dacitic compositions and the whole volcanics were produced by melting of ca. 2 Ga orthogneissic basement rocks in a rift or back-arc tectonic setting.

Mineralogically, the metasomatic alteration is marked by incipient to total adularization of primary phenocrysts of monoclinic K-feldspar (total), of plagioclase (incipient to total), as well as of feldspars in the matrix (total). This is observed both in deformed rocks and their undeformed counterparts. In undeformed rocks beneath the nappe, adularia is identified by its morphology and microprobe analysis (Le Hébel, ms, 2002). Microstructures show that adularization was favored by initial cracks and cleavages and led to the disappearance of any previous twins, cracks, or zoning structures that are only preserved in relict primary feldspar islands. Metasomatic adularization resulted in an increase of K/Na ratios (fig. 9) and losses of Ca (brine circulation ?).

Quartz and feldspar phenocrysts or clasts and the matrix itself are impregnated with a fine opaque graphitic dust (example, figs. 3A-D). In undeformed rocks, the graphitic dust is seen to be concentrated as laminae parallel to the primary (magmatic)

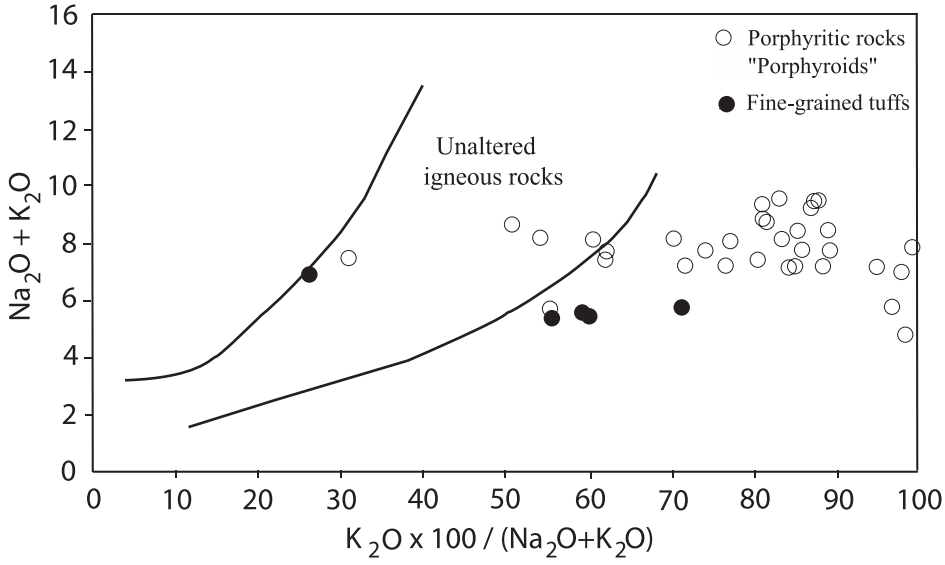


Fig. 9. Whole rock chemical compositions of the metavolcanics from the Porphyroid nappe plotted in the Hughes (1973) diagram. Non disturbed magmatic rocks should plot between the two curves. This diagram demonstrates that most of the studied porphyritic rocks and fine-grained tuffs are metasomatized and display highly disturbed Na/K ratios.

layering or as dots located at grain boundaries in the matrix and suggesting (Parnell, personal communication) ancient oil droplets. In quartz, the graphitic dust is only found in more or less cemented cracks (inclusion planes, fig. 3C). In feldspar phenocrysts (macroscopically black-colored), the graphitic dust is finely distributed as "fishback bones" (migration along cracks and cleavages, fig. 3D). All these observations argue for an input of organic matter as a liquid phase (oil), a hypothesis that is supported by the low and similar carbon isotopic compositions of graphite from both volcanics and spatially associated black shales. Indeed, during oil extraction and subsequent pyrolysis (maximum temperature reached = 350 – 400°C, Le Hébel and others, 2002b), the $^{13}C/^{12}C$ ratio of kerogen is relatively preserved or slightly enriched (example, Simoneit and others, 1981; Andresen and others, 1995; see also Des Marais, 2001, and references therein). Thus, the $^{13}C/^{12}C$ ratios of the black shales are comparable with those of the marine organic carbon found in the Silurian and Devonian sediments from the western Variscan orogen (Lécuyer and Paris, 1997). Generally, the carbon isotopic signature of crude oil is akin or slightly $^{13}C$-depleted compared to that of the related source kerogen, and this isotopic similarity should not be affected by subsequent pyrolysis (example, Arneth and Matzigkeit, 1986). The input of organic matter occurred when feldspars still had a high porosity (probably due to alteration) that was subsequently reduced by recrystallization associated with K-metasomatism. This is supported by the disappearance of cracks and cleavages in feldspars that suffered adularization. We conclude that oil impregnation occurred prior to (or partly during) adularization.

During deformation and metamorphism, adularia is no longer stable. The small crystals (matrix) and parts of the adularized phenocrysts or clasts were transformed into microcline or into chessboard albite. Moreover, in pressure shadows, feldspar neoblasts are limpid microcline (fig. 10) or, rarely, small albite crystals.

Thus, metasomatic alteration with large changes in K, Na, Ca contents occurred prior to deformation and metamorphism, necessarily under large fluid/rock ratios and it was preceded or accompanied by oil migration (fig. 5). The anomalously

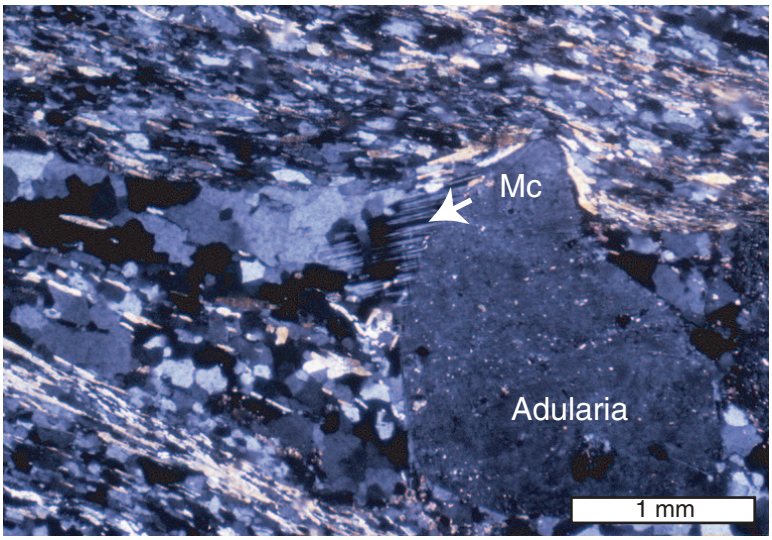


Fig. 10. Syn-kinematic microcline in a pressure shadow around an adularitized feldspar porphyroclast (XPL). Microcline is the syn-kinematic K-feldspar species and postdates adularization of former feldspar phenocrysts.

$^{18}$O-rich WR compositions are likely to be associated with this metasomatic event. Uncertainties on the mineralogical compositions and temperatures of equilibration during metasomatism preclude precise estimates of the corresponding fluid O isotopic signature.

### *Reconstruction of the P-T Evolution*

Reconstruction of the P-T path has been carried out using fluid inclusion isochores representative of each type of fluid (fig. 11). Total homogenization temperatures Th or decrepitation temperatures indicate minimal trapping temperatures from 270 to 370°C in inclusions from deformed metavolcanics of the Porphyroid nappe. Maximum trapping temperatures are estimated to be around 400°C. Such peak thermal conditions are consistent with the stability of chlorite and the lack of biotite. Furthermore, thermodynamic models of phengite-chlorite assemblages using the methods developed by Vidal and others (2001) have yielded peak metamorphic conditions of 350 ± 50°C for pressures of 800 ± 100 MPa (Le Hébel and others,

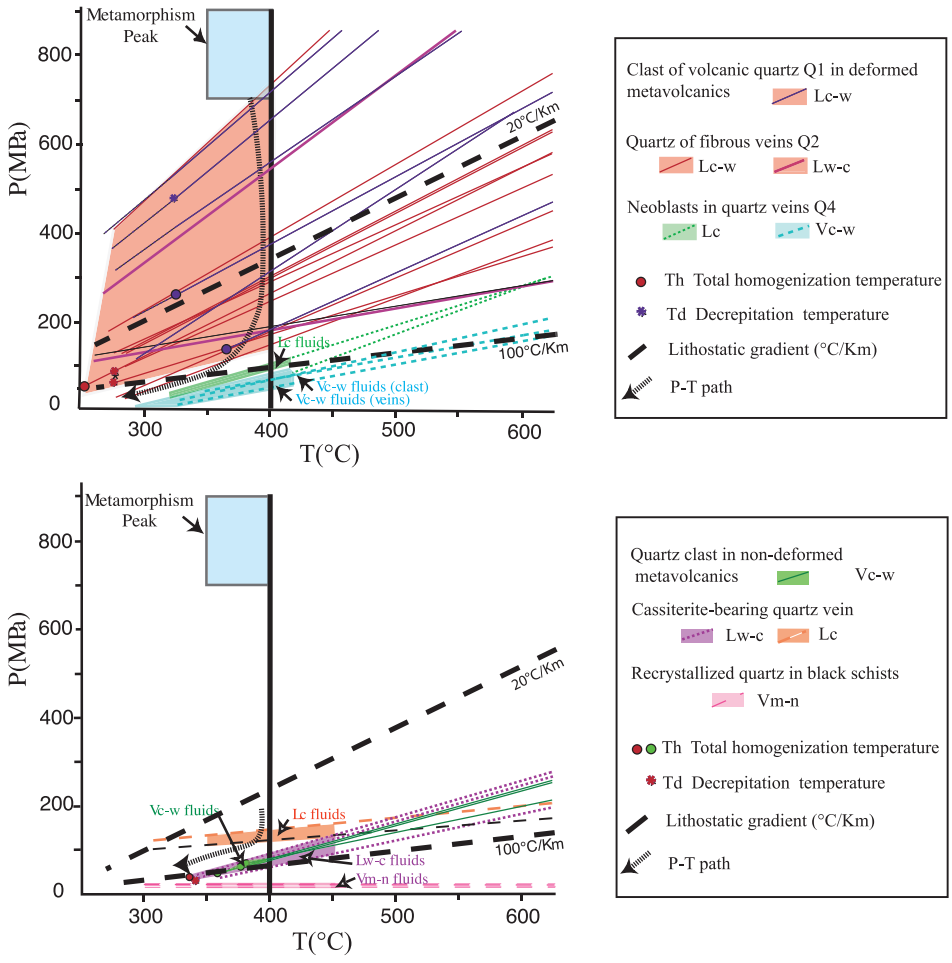


Fig. 11. Pressure-temperature reconstruction of the conditions prevailing in the studied zones of the Porphyroid nappe unit (see text for comments).

2002b). Using the isochores of highest-density fluid inclusions, maximum fluid trapping pressures are consistently estimated to be around 750 MPa. The presence of annular and semi-annular inclusions in quartz volcanic clasts (fig. 4 B) further attests to high pressure conditions (Pêcher, 1981; Boullier and others, 1991). The lowest-density fluid inclusion isochores provide minimal fluid trapping pressures below 100 MPa for temperatures around 300°C, which may suggest a high apparent geothermal gradient (up to 100°C/km) at that trapping stage. In summary, fluid trapping P-T conditions in the Porphyroid nappe are consistent with a nearly isothermal retrograde path (between 400 and 300°C), which suggests a rather fast exhumation of the unit. This is in agreement with geochronological data obtained on the overlying blueschists from the Ile de Groix that also suggest rapid exhumation (Bosse and others, 2005).

All fluid inclusions from the non-deformed porphyritic lavas beneath the nappe have flat isochores with minimal trapping temperatures of 370° to 390°C, in the same range as those estimated in the nappe. Trapping pressure estimates are 50 and 100 MPa, corresponding to 3 to 4 Km depth, which again, might suggest a high geothermal gradient (up to 100°C/Km). Low trapping pressures are also consistent with the lack of any decrepitated or semi-annular inclusions. All these features indicate that porphyritic lavas beneath the nappe did not undergo or did not record a high pressure event. Nevertheless, aqueous-carbonic fluid compositions in the Porphyroid nappe and in porphyritic lavas beneath the nappe are similar.

Fluids from the cassiterite quartz veins at the roof of the Guérande granite are trapped at temperatures ranging from 350 to 450°C and pressures between 50 and 150 MPa. The lowest P-T pairs for such fluids are close to the immiscibility boundary, which explains the occurrence of volatile-dominated inclusions with no visible water but containing frequently up to a few percent of water, as shown by Raman spectroscopy. These are typical of the rather high temperatures, which prevailed at shallow depth in areas of the Variscan basement that were marked by intrusion of peraluminous granites and U mineralizations around 300 to 310 Ma (Cathelineau and others, 1990). Similar P-T conditions are recorded in the quartz from black shales on top of the Guérande granite where $CH_4$-$N_2$ fluids issued from devolatilization processes were trapped at very low pressure (20 – 30 MPa). Such pressures could be interpreted as hydrostatic pressures prevailing at shallow depths (2 – 3 km) during - or immediately after - the granite intrusion.

The flat slopes of isochores found at the roof of the Guérande granite are associated with a local intrusion-induced temperature increase at shallow emplacement depth. In contrast, such interpretation cannot hold for the flat isochores slopes (fig. 11A) observed within the volcanics beneath the Porphyroid nappe where no late granitic intrusion is known. There, high temperatures at shallow depth cannot either reflect a high geotherm associated with any kind of reasonable tectonic context. Indeed, late deformations beneath the nappe relate to crustal-scale extension marked by downward increases of pressure, temperature and strain (Cagnard and others, 2004). The samples studied here are located at the top of the metamorphic pile, at some 4 to 5 km above the biotite-in isograd within metapelites, and in an upper crustal level where the extensional reworking is absent or minimum (Goujou, ms, 1992; Cagnard and others, 2004). Thus, the best explanation for the high temperatures observed at such a shallow level is a local heat input from the directly overlying porphyroid nappe during its emplacement.

### *Synkinematic Fluid Regime*

*Initial fluid migration.*—Prior to deformation, the 480 to 490 Ma-old calc-alkaline volcanic protoliths of the Vendée metavolcanics were deposited in a coastal (continental + marine) environment. Initially, these rocks certainly possessed a high porosity (see estimates for such rocks by Sruoga and others, 2004). They were strongly hydrated

through low-temperature fluid/rock interactions, as shown by their anomalously high K contents and O isotopic ratios, and experienced oil migration. Processes of oil migration are well documented in both extensional and compressional contexts (example, Larroque and others, 1996; Moretti and others, 2002, and references therein; Parris and others, 2003, and references therein), with oil-window temperatures on the order of 80 to 160°C (example, Hunt, 1996). On the other hand, the temperature of K-metasomatism is poorly constrained. Adularia is known to crystallize in a wide range of conditions, from sub-surface temperatures (example, Jorgensen, 1981) to much higher ones (example, Walgenwitz and others, 1990; Fulignati and others, 1997; Ennis and others, 2000; Boyce and others, 2003). High temperature adularia is especially observed for rocks of high K/K+Na+Ca chemistry, such as the pegmatoid veins located within the Vendée metavolcanics (350 – 400°C, Le Hébel and others, 2002a). In the metavolcanics, textural relationships show that adularia grew after oil migration but prior to deformation and metamorphism. Indeed, adularia is impregnated with organic matter whereas it is partly replaced by graphite-free microcline during deformation and microcline is the stable K-feldspar in shadow-zones (fig. 10). Thus, it is tempting to see oil migration and K-metasomatism to be sub-coeval (fig. 5). K-metasomatism is known in extensional settings (example, Brooks, 1986; Roddy and others, 1988). Moreover, replacement adularia hosting oil droplets is known in oil reservoirs located in coastal basins at passive margins (Walgenwitz and others, 1990). On the other hand, the black shales associated with the metavolcanics contain graphitized microfossils that suggest an age close to the Silurian-Devonian boundary (Peucat and others, 1986). Silurian formations are known to be the main Palaeozoic oil source worldwide. From this, we may reasonably infer that oil migration into the metavolcanics should be younger than the Silurian. Recent Rb-Sr and $^{39}Ar$-$^{40}Ar$ analyses indicate that the age of the HP-LT blueschist metamorphism in the area (Ile-de-Groix and Bois de Céné, fig. 1A) is ca. 360 to 370 Ma (Bosse and others, 2005), an age also found in some phengites from the Porphyroid nappe (laser $^{40}Ar/^{39}Ar$ dating, Ruffet, work in progress; Le Hébel, ms, 2002). Thus, oil migration and K-metasomatism likely occurred during the Lower to Middle Devonian.

The fact that the present-day imbrication of Silurian black shales and Lower Ordovician volcanics necessarily results from thrust tectonics does not straightforwardly imply that the process of oil migration relates to that context. Three hypotheses may be invoked for oil migration context from a source-rock towards older rocks. Downward limited migration might be eventually evoked if upward motion was inhibited by overlying impermeable layers. However, much more likely is upward or lateral migration either in extensional or compressional contexts with juxtaposition of young rocks and older ones by block tilting or thrusting, respectively. Important block tilting should preferentially mark the early stages of rifting-type extension. In the Hercynian belt of Brittany, the onset of the major rifting event and associated block-tilting occurred during Lower Ordovician times (Brun and others, 1991), that is more than 50 Ma before the deposition of the Silurian potential source rocks. This latter period is most likely characterized by a context of stable passive margin. Thus, from the above arguments, we propose that oil migration and K-metasomatism were related to the onset of syn-convergence compression during the Devonian. This episode might mark the onset of the major compressional event that brought the volcanic material into a HP-LT prograde path. Examples are known in which tectonic thickening and gas-overpressures inducing hydraulic fracturing may lead to oil or gas migration (example, Ferket and others, 2003; Parris and others, 2003). The sequence of events that affected the metavolcanics from the Porphyroid nappe is summarized in figure 5.

*Fluid confining during the metamorphic history.*—As summarized previously, Le Hébel (ms, 2002), Le Hébel and others (2002a) have developed several structural, mineralogical and geochemical lines of evidence showing that deformations observed within the Porphyroid nappe accumulated by combined crack-sealing and dissolution-crystallization involving quartz and feldspars in a system closed to fluids under low fluid/rock ratios. From these, they argued that dissolution-crystallization was mainly driven by diffusion rather than by advection. In addition, the observed distributed and coeval ductile and brittle deformation mechanisms led these authors to infer that fluid and lithostatic pressures were probably of comparable magnitudes.

Additional data presented in this paper, in particular fluid inclusion compositions and carbon isotopes further support - or are consistent with - a system basically closed to fluids. Indeed, fluid inclusions within the nappe do not show important compositional variations irrespective of the nature of host-quartz and host-rock. They systematically belonged to the C-H-O-N system and contained $H_2O$, $CO_2$ and minor volatile components such as $CH_4$. The spectacular preservation of graphitic matter in large portions of the Porphyroid nappe and the rather homogeneous $\delta^{13}C$-values of that graphite argue that the rocks buffering capacity of carbon isotopic compositions was never exceeded during deformation as previously shown for oxygen isotopes (Le Hébel and others, 2000, 2002a).

Compared to the largely open fluid regime that prevailed during the early history of the metavolcanics from the Porphyroid nappe, their subsequent tectonic evolution shows a very different behavior. The occurrence of large and distributed strains without evidence of strain localization and fluid advection (Le Hébel and others, 2002a) is a very uncommon situation at such low temperatures in feldspar-rich lithologies. In New Brunswick, for example, rocks with comparable compositions, initial textures and P-T-t paths, show evidence of strain localization (Van Staal and others, 2001). These authors attributed the observed heterogeneous deformation pattern to metasomatic weakening via albite formation during low-temperature, large-scale opening to externally-derived fluids. In contrast, in our example, strains are distributed throughout both albite-bearing rocks and K-feldspar-bearing ones. Differences between deformation modes in the Porphyroid nappe and in the New Brunswick example (Van Staal and others, 2001) imply that neither the occurrence of albite nor the HP/LT metamorphic path are key factors controlling the degree of strain localization. They instead underline the major role of the nature of fluid/rock interaction that may vary, in principle, from an open fluid system dominated by advection to a closed system dominated by diffusion. The initial high porosity of our volcanic protoliths may be the key factor that induced the subsequent distribution mode. Indeed, beside introducing replacement adularia and oil, early metasomatic alteration likely produced significant amounts of clay minerals in the protoliths (hydration of volcanic glass in a porous pyroclastic material). Thus, in contrast to a granitic protolith where water introduction is a major weakening factor leading to strain localization, an initially significant and distributed amount of internal water source may account for the lack of strain localization. In such an interpretation, the Porphyroid nappe appears as a potential fluid source rather than a sink or a pathway for external fluids during its tectonic history. The early occurrence of oil and its maturation might have been additional features that inhibited the input of external water. Indeed, pyrolysis of organic matter is known to induce transient gas overpressures with hydraulitic fracturing (followed by fracture cementation) during tectonic burial of sediments (200 – 250°C, 10 km-depth, example, Parris and others, 2003). Subsequently, high internal fluid pressures might have been maintained in localized volumes through protracted oil pyrolysis and via reactions such as C (graphite = pyrolyzed oil) + $H_2O \rightarrow CO_2 + CH_4$. Diffusion-dominated dissolution-crystallization,

as well as grain-scale and aggregate-scale cracking mechanisms that characterize the deformation of our metavolcanics indicate limited fluid migration. Thus, the observed deformation mode, quite uncommon in LT felsic rocks, is not only related to the primary occurrence of distributed fluids, but may in turn account for their long-lasting trapping through small cyclic jumps triggered by continuous cracking and sealing (Etheridge and others, 1984).

## CONCLUDING REMARKS

Low-temperature deformation of quartz-feldspar rocks, like granitoids, is in general marked by strong strain localization along discrete shear zones. This feature is often associated with channelled influx of externally-derived water-rich fluids inducing reaction softening through feldspar-to-mica transformation and through albitization of K-feldspar and plagioclase. Based on structural, microstructural and geochemical data, Le Hébel and others (2002a) have documented a deformation mode in the felsic metavolcanites from the Porphyroid nappe that is very uncommon for felsic rocks at low-temperature, a deformation mode marked by large distributed strains accommodated by dissolution-crystallization and crack-sealing. This occurred probably because of distributed high-fluid pressures induced by the permanent and penetrative presence of an early fluid phase under low fluid/rock ratios. The present study confirms these conclusions. Moreover, it emphasizes the prominent role played by initial metasomatism in the development of this original deformation mode. Hydration, more or less coeval with extensive alkali metasomatism and with oil input, ascribed a hydrated composition to felsic lithologies that usually are rather devoid of water (granitoids). The Porphyroid nappe crops out for more than 200 kms from Brittany to Vendée with similar pervasive strains. The formation of this large ductile body is the consequence of a primary pervasive wetting of a rock system that "stewed in its own juice" during the subsequent progressive deformation history. Thus, although the Porphyroid nappe may, at first sight, appear as an opposite end-member to the common process of water-induced strain softening and localization, it may be regarded, as a whole, as a water-weakened deformation zone at crustal-scale.

## ACKNOWLEDGMENTS

This work was in part supported by the Géofrance 3D BRGM-CNRS program (Armor2 project). The paper greatly benefited from careful and constructive reviews by R. Burruss, R. Worden and an anonymous reviewer.

## Appendix. Analytical Techniques

### *A 1. Stable Isotopes (Géosciences Rennes)*

O isotopic compositions were measured on whole rocks and silicate minerals by reacting 5 to 10 mg of sample with $BrF_5$ at 650°C in Ni reaction vessels (Clayton and Mayeda, 1963), converting $O_2$ into $CO_2$. Reduced carbon (graphitic dust) was quantitatively oxidized into $CO_2$ with purified CuO in sealed silica glass tubes. All the isotopic ratios were measured on $CO_2$ gas using a VG SIRA 10 instrument. In addition to the use of internal standards (basaltic MORB glass and granite standard), the reference materials used to calibrate the analytical procedures are NBS 28 (O silicates), NBS 19 (O, C), USGS 24 (C). The NBS 28 $\delta^{18}O$ values found during the 2 main experimental periods of this study were 9.37 ± 0.11 permil (n=15) and 9.10 ± 0.06 permil (n=7). O isotopic measurements on silicates were thus normalized to a NBS 28 value of 9.6 permil. The $\delta^{13}C$-value of the USGS 24 graphite material found during the course of the study (oxidation with CuO technique) was –15.97 ± 0.06 permil (n=3) with respect to the NBS 29 carbonate calibration. All the data are expressed as permil versus SMOW (O) and PDB (C) and, on the basis of duplicate extractions and mass spectrometry measurements, typical uncertainties are estimated to be on the order of 0.15 permil (O) and 0.05 permil (C).

### *A 2. Fluid Inclusions (G2R/CREGU, Nancy)*

P-T-V-X characterization of fluids was obtained through a multidisciplinary study of fluid inclusions by techniques that included microthermometry and quantitative *in-situ* analysis of gases by Raman spectros-

copy. Microthermometric studies were performed on wafers using a Chaixmeca heating-freezing stage (Poty and others, 1976). The stage was calibrated with melting-point standards at T>25°C and natural and synthetic fluid inclusions at T< 0°C. The rate of heating was monitored in order to obtain an accuracy of ± 0.2°C during freezing, ±1°C when heating over the range 25 to 400°C. Salinity, expressed as weight percent NaCl eq., was calculated from microthermometric data using equations from Bodnar (1983).

In volatile-bearing fluid inclusions, $CO_2$ was identified by melting of a solid below -56.6°C and/or by presence of clathrates at low temperatures. The volume fraction of the aqueous liquid and the volume fraction of the volatile-rich liquid ($CO_2$ dominated liquid) in the volatile-rich phase have been estimated at room temperature by reference to the volumetric chart of Roedder (1984).

Molar fractions of $CO_2$, $CH_4$, $H_2S$ and $N_2$ were determined in individual fluid inclusions by micro-Raman analysis performed on Labram (Dilor) Raman spectrometer at G2R laboratory (Nancy) following the procedure given by Dubessy (1984) and Dubessy and others (1989). Molar fraction of NaCl, molar volume and bulk compositions were determined by combining results from microthermometry, Raman analysis results, and using calculation codes (Bakker, 1997). The P-T properties were modeled using the V-X data and the equation of state of Bowers and Helgeson (1983), reviewed by Bakker (1999).

## REFERENCES


Andresen, B., Throndsen, T., Råheim, A., and Bolstad, J., 1995, A comparison of pyrolysis products with models of natural gas generation: Chemical Geology, v. 126, p. 261–280.

Arneth, J. D., and Matzigkeit, U., 1986, Laboratory-simulated thermal maturation of different types of sediments from the Williston Basin, North America – Effects on the production rates, the isotopic and organo-geochemical composition of various pyrolysis products: Chemical Geology (Isotope Geoscience Section), v. 58, p. 339–360.

Audren, C., and Jégouzo, P., 1986, 1/50,000-scale geological map "Belle-Ile-En-Mer, Houat, Hoedic", N° 447-477: BRGM Ed., Orléans, France.

Audren, C., and Triboulet, C., 1993, P-T-t-deformation paths recorded by kinzigites during diapirism in the western Variscan belt (Golfe du Morbihan, southern Brittany, France): Journal of Metamorphic Geology, v. 11, p. 337–356.

Bakker, R. J., 1997, Clathrates: computer programs to calculate fluid inclusion V-X properties using clathrate melting temperatures: Computers and Geosciences, v. 23, p. 1–18.

——— 1999, Adaptation of the Bowers and Helgeson (1983) equation of state to the $H_2O$-$CO_2$-$CH_4$-$N_2$-NaCl system: Chemical Geology, v. 154, p. 225–236.

Baumgartner, L. P., and Valley, J. W., 2001, Stable isotope transport and contact metamorphism fluid flow, *in* Valley, J. W., and Cole, D. R., editors, Stable isotope geochemistry: Mineralogical Society of America, Reviews in Mineralogy, v. 43, p. 415–468.

Bernard-Griffiths, J., Peucat, J. J., Sheppard, S. M. F., and Vidal, P., 1985, Petrogenesis of Hercynian leucogranites from South Armorican Massif. Contributions of REE and isotopic (Sr, Nd, Pb,O) geochemical data to the study of source rocks characteristics and ages: Earth and Planetary Science Letters, v. 74, p. 235–250.

Bodnar, R. J., 1983, A method of calculating fluid inclusions volumes based in vapor bubble diameter and P-V-T-X properties on inclusions fluid: Economic Geology, v. 78, p. 535–542.

Boiron, M. C., Essaraj, S., Sellier, E., Cathelineau, M., Lespinasse, M., and Poty, B., 1992, Identification of fluid inclusions in relation with their host microstructural domains in quartz by cathodoluminescence: Geochimica et Cosmochimica Acta, v. 56, p. 175–185.

Boiron, M. C., Cathelineau, M., Banks, D. A., Fourcade, S., and Vallance, J., 2003, Mixing of metamorphic and surficial fluids during the uplift of the Hercynian upper crust: consequences for gold deposition: Chemical Geology, v. 194, p. 119–141.

Bosse, V., Ballèvre, M., and Vidal, O., 2002, Ductile thrusting recorded by the garnet isograd from the blueschist-facies metapelites of the Ile de Groix, Armorican Massif, France: Journal of Petrology, v. 43**,** p. 485–510.

Bosse, V., Féraud G., Ballèvre, M., Peucat, J. J., and Corsini, M., 2005, Rb-Sr and $^{40}Ar/^{39}Ar$ ages in the blueschists from the Ile-de-Groix (Armorican Massif, France): implications for closure temperatures: Chemical Geology, v. 220, 1–2, p. 21–45.

Boullier, A., France-Lanord, C., Dubessy, J., Adamy, J., and Champenois, M., 1991, Linked fluid and tectonic evolution in the High Himalaya mountains (Nepal): Contributions to Mineralogy and Petrology, v. 107, p. 358–372.

Bowers, T. S., and Helgeson, H. C., 1983, Calculation of the thermodynamic and geochemical consequences of non-ideal mixing in the system $H_2O$-$CO_2$-NaCl on phase relations in geologic systems: metamorphic equilibria at high pressures and temperatures: American Mineralogist, v. 68, p. 1059–1075.

Boyce, A., Fulignati, P., and Sbrana, A., 2003, Deep hydrothermal circulation in a granite intrusion beneath Larderello geothermal area (Italy): constraints from mineralogy, fluid inclusions and stable isotopes: Journal of Volcanology and Geothermal Research, v. 126, 3–4, p. 243–262.

Brooks, W. E., 1986, Distribution of anomalously high $K_2O$ volcanic rocks in Arizona: Metasomatism at the Picacho Peak detachment fault: Geology, v. 14, p. 339–342.

Brown, M., and Dallmeyer, R. D., 1996, Rapid Variscan exhumation and the role of magma in core complex formation: southern Brittany metamorphic belt, France: Journal of Metamorphic Geology, v. 14, p. 361–379.

Brun, J. P., and Burg, J. P., 1982, Combined thrusting and wrenching in the Ibero-Armorican arc: a corner effect during continental collision: Earth and Planetary Science Letters, v. 61, p. 319–332.
Brun, J. P., Ballard, J. F., and Le Corre, C., 1991, Identification of Ordovician block-tilting in the Hercynian fold belt of central Brittany: field evidence and computer models: Journal of Structural Geology, v. 13, p. 419–429.
Burg, J. P., 1981, Tectonique tangentielle hercynienne en Vendée littorale: Signification des linéations d'étirement E-W dans les porphyroïdes à foliation horizontale: Comptes Rendus de l'Académie des Sciences de Paris, série II, v. 293, p. 849–854.
Cagnard, F., Gapais, D., Brun, J. P., Gumiaux, C., and Van den Driessche, J., 2004, Late pervasive crustal-scale extension in the south Armorican Hercynian belt (Vendée, France): Journal of Structural Geology, v. 26, 3, p. 435–444.
Cathelineau, M., Boiron, M. C., Holliger, P., and Poty, B., 1990, Metallogenesis of the French part of the Variscan orogen. Part II: Time-space relationships between U, Au and Sn-W ore deposition and geodynamic events - Mineralogical and U-Pb data: Tectonophysics, v. 177, p. 59–79.
Clayton, R. N., and Mayeda, T. K., 1963, The use of bromine pentafluoride in the extraction of oxygen from oxides and silicates for isotopic analysis: Geochimica et Cosmochimica Acta, v. 27, p. 43–52.
Des Marais, D. J., 2001**,** Isotopic evolution in Precambrian biogeochemical carbon cycle, *in* Valley, J.W., and Cole, D. R., editors, Stable isotope geochemistry: Mineralogical Society of America, Reviews in Mineralogy, v. 43, p. 555–578.
Dipple, G. M., and Ferry, J. M., 1992, Metasomatism and fluid flow in ductile fault zones: Contributions to Mineralogy and Petrology, v. 112, 2–3, p. 149–164.
Dubessy, J., 1984, Simulations des équilibres chimiques dans le système C-O-H conséquence méthodologique pour les inclusions fluides: Bulletin de Minéralogie, v. 107, p. 157–168.
Dubessy, J., Poty, B., and Ramboz, C., 1989, Advances in C-O-H-N-S fluid geochemistry based on micro-Raman spectrometric analysis of fluid inclusions: European Journal of Mineralogy, v. 1, p. 517–534.
Dubessy, J., Boiron, M. C., Moissette, A., Monin, C., and Sretenskaya, N., 1992, Determinations of water, hydrates and pH in fluid inclusions by micro-Raman spectrometry: European Journal of Mineralogy, v. 4, p. 885–894.
Ennis, D. J., Dunbar, N. W., Campbell, A. R., and Chapin, C. E., 2000, The effects of K-metasomatism on the mineralogy and geochemistry of silicic ignimbrites near Socorro, New Mexico: Chemical Geology, v. 167, p. 285–312.
Etheridge, M. S., Wall, V. J., Cox, S. F., and Vernon, R. H., 1984, High fluid pressures during metamorphism and deformation: implications for mass transport and deformation mechanisms: Journal of Geophysical Research, v. 89, p. 4,344–4,358.
Ferket, H., Swennen, R., Ortuño, S., and Roure, F., 2003, Reconstruction of the fluid flow history during Laramide forelandfold and thrust belt development in eastern Mexico: cathodoluminescence and $\delta^{18}O$–$\delta^{13}C$ isotope trends of calcite-cemented fractures: Journal of Geochemical Exploration, v. 78–79, p. 163–167.
Ferry, J. M., 1994. Historic review of metamorphic fluid flow: Journal of Geophysical Research, v. 99, B8, p. 15,487–15,498.
Fourcade, S., Capdevila, R., Ouabadi, A., and Martineau, F., 2001, The origin and geodynamic significance of the Alpine cordierite-bearing granitoids of northern Algeria. A combined petrological, mineralogical, geochemical and isotope (O, H, Sr, Nd) study: Lithos, v. 57, p. 187–216.
Fulignati, P., Malfitano, G., and Sbrana, A., 1997, The Pantelleria caldera geothermal system: Data from the hydrothermal minerals: Journal of Volcanology and Geothermal Research, v. 75, 3–4, p. 251–270.
Fyfe, W. S., Price, N. J., and Thompson, A. D., 1978, Fluids in the earth's crust: Amsterdam, Elsevier, 383 p.
Gapais, D., 1989, Shear structures within deformed granites: thermal and mechanical indicators: Geology, v. 17, p. 1,144–1,147.
Gapais, D., Lagarde, J. L., Le Corre, C., Audren, C., Jegouzo, P., Casas Sainz, A., and Van Den Driessche, J., 1993, La zone de cisaillement de Quiberon: témoin d'extension de la chaîne varisque en Bretagne méridionale au Carbonifère: Comptes Rendus de l'Académie des Sciences de Paris, Série II, v. 316, p. 1,123–1,129.
Goujou, J. C., ms, 1992, Analyse pétro-structurale dans un avant-pays métamorphique: influence du plutonisme tardi orogénique varisque sur l'encaissant epi à mézozonal de Vendée: Montpellier, France, Université de Montpellier 2, Thesis, 347 p.
Gueydan, F., Leroy, Y. M., Jolivet, L., and Agard, P., 2003, Analysis of continental mid-crustal strain localisation induced by reaction-softening and microfracturing: Journal of Geophysical Research, v. 108, p. 2,064, doi:10.1029/2001JB000611.
Hugues, C. J., 1973, Spilites, keratophyres and the igneous spectrum: Geological Magazine, v. 109, p. 513–527.
Huizenga, J. M., 2001, Thermodynamic modelling of C-O-H fluids: Lithos, v. 55, p. 101–114.
Iglesias, M., and Brun, J. P., 1976, Signification des variations et anomalies de la déformation dans un segment de la chaîne hercynienne (les séries cristallophylliennes de la Vendée littorale, Massif Armoricain): Bulletin de la Société Géologique de France, v. 7, p. 1,443–1,452.
Hunt, J. M., 1996, Petroleum Geochemistry and Geology: New York, W. H. Freeman and Company, 743 p.
Jones, K. A., and Brown, M., 1990, High-temperature "clockwise" P-T paths and melting in the development of regional migmatites: an example from Southern Brittany, France: Journal of Metamorphic Geology, v. 14, p. 361–379.
Jorgensen, N. O., 1981, Authigenic K-feldspar in recent submarine gypsum concretions from Denmark: Marine Geology, v. 39, 1-2, p. 21–15.
Kretz, R., 1983, Symbols for rock-forming minerals: American Mineralogist, v. 68, p. 277–279.
Kyser, T. K., and Kerrich, R., 1990, Geochemistry of fluids in tectonically active crustal regions, *in* Nesbitt, B. E., editor, Fluids in tectonically active regimes of the continental crust: Mineralogical Association of Canada, v. 18, p. 133–230.

Larroque, C., Guilhaumou, N., Stephan J. F., and Roure, F., 1996, Advection of fluids at the front of the Sicilian Neogene subduction complex: Tectonophysics, v. 254, 1-2, p. 41–55.
Lécuyer, C., and Paris, F., 1997, Variations in the $\delta^{13}C$ of lower Paleozoic palynomorphs: implications for the interpretation of ancient marine sediments: Chemical Geology, v. 138, p. 161–170.
Le Hébel, F., ms, 2002, Déformation continentale et histoire des fluides au cours d'un cycle subduction, exhumation, extension. Exemple des porphyroïdes sud-armoricains: Rennes, France, Université de Rennes, Ph. D. thesis, 254 p.
Le Hébel, F., Fourcade, S., Gapais, D., Marignac, C., Capdevila, R., and Martineau, F., 2000, Fluid-assisted spreading of thickened continental crust: Preliminary data from the Variscan Belt of South Brittany: Journal of Geochemical Exploration, v. 69–70, p. 561–564.
Le Hébel, F., Gapais, D., Fourcade, S., and Capdevila, R., 2002a, Fluid-assisted large strains in a crustal-scale décollement (Hercynian belt of South Brittany, France), *in* De Meer, S., Drury, M. S., De Bresser, J. H. P., and Pennock, G. M., editors, Deformation mechanisms, rheology and tectonics: current status and future perspectives: London, Geological Society, Special Publication, v. 200, p. 85-101.
Le Hébel, F., Vidal, O., Kiénast, J. R., and Gapais, D., 2002b, Les Porphyroïdes de Bretagne méridionale: une unité de HP-BT dans la chaîne Hercynienne. Evidence for HP-LT Hercynian metamorphism within the "porphyroïdes" of South Brittany (France): Comptes-Rendus des Géosciences, v. 334, p. 205–211.
Moretti, I., Labaume, P., Sheppard, S. M. F., and Boulègue, J., 2002, Compartmentalisation of fluid migration pathways in the sub-Andean Zone, Bolivia: Tectonophysics, v. 348, 1–3, p. 5–24.
Munha, J., Fyfe, W. S., and Kerrich, R., 1980, Adularia, the characteristic mineral of felsic spilites: Contributions to Mineralogy and Petrology, v. 75, p. 15–19.
Oliver, N. H. S., 1996, Review and classification of structural controls on fluid flow during regional metamorphism: Journal of Metamorphic Geology, v. 14, p. 477–492.
O'Neil, J. R., and Chappell, B. W., 1977, Oxygen and hydrogen isotope relations in the Berridale batholith: London, Journal of the Geological Society, v. 133, p. 559–571.
Parris, T. M., Burruss, R. C., and O'Sullivan, P. B., 2003, Deformation and the timing of gas generation and migration in the eastern Brooks range foothills, Arctic National Wildlife Refuge, Alaska: The American Association of Petroleum Geologists Bulletin, v. 87, 11, p. 1,823–1,846.
Pêcher, A., 1981, Experimental decrepitation and reequilibration of fluid inclusions in synthetic quartz: Tectonophysics, v. 78, p. 567–584.
Peucat, J. J., Paris, F., and Chalet, M., 1986, U-Pb zircon dating of volcanic rocks, close to the Silurian-Devonian boundary, from Vendée (western France): Chemical Geology (Isotope Geoscience Section), v. 59, p. 133–142.
Poty, B., Leroy J., and Jachimowicz, L., 1976, Un nouvel appareil pour la mesure des températures sous le microscope, l'installation de la microthermométrie Chaixmêca: Bulletin de la Société Française de Minéralogie, v. 99, p. 182–186.
Roddy, M. S., Reynolds, S. J., Smith, B. M., and Ruiz, J., 1988, K-metasomatism and detachment-related mineralization, Harcuvar Mountains, Arizona: Geological Society of America Bulletin, v. 100, p. 1,627–1,639.
Roedder, E., 1984, Fluid inclusions, *in* Ribbe, P., series editor: Mineralogical Society of America, Reviews in Mineralogy, v. 12, 644 p.
Schulz, B., Audren, C., and Triboulet, C., 2001, Oxygen isotope record of fluid-rock $SiO_2$ interaction during Variscan progressive deformation and quartz veining in the meta-volcanosediments of Belle-Ile (Southern Brittany): Journal of Structural Geology, v. 24, 8, p. 1,281–1,297.
Simoneit, B. R. T., Brenner, S., Peters, K. E., and Kaplan, I. R., 1981, Thermal alteration of Cretaceous black shale by diabase intrusions in the Eastern Atlantic: II Effects on bitumen and kerogen: Geochimica et Cosmochimica Acta, v. 45, p. 1,581–1,602.
Sruoga, P., Rubinstein, N., and Hinterwimmer, G., 2004, Porosity and permeability in volcanic rocks: a case study on the Serie Tobifera, South Patagonia, Argentina: Journal of Volcanology and Geothermal Research, v. 132, p. 31–43.
Talbert, J. C., and Vialette, Y., 1972, Etude géochronologique du massif de Mareuil-sur-Lay (Vendée): Comptes Rendus de l'Académie des Sciences de Paris, v. 274, p. 2,737–2,739.
Tecce, F., Rosetti, F., and Funiciello, R., 2001, Re-equilibration textures of fluid inclusions in exhumed high-pressure rocks: the example of the Tuscan Archipelago (Northern Tyrrhenian Sea, Italy): Mineralogy and Petrology, v. 71, p. 139–147.
Ters, M., 1972, Geological map Palluau-Ile d'Yeu: Bureau de Recherches Géologiques et Minières, n° 129, 2nd édition, scale 1/80,000.
Van Staal, C. R., Rogers, N., and Taylor, B. E., 2001, Formation of low-temperature mylonites and phyllonites by alkali-metasomatic weakening of felsic volcanic rocks during progressive, subduction-related deformation: Journal of Structural Geology, v. 23, p. 903–921.
Vauchez, A., Maillet, D., and Sougy, J., 1987, Strain and deformation mechanisms in the Variscan nappes of Vendée, South Brittany, France: Journal of Structural Geology, v. 9, p. 31–40.
Vidal, O., Parra, T., and Trotet, F., 2001, A thermodynamic model for Fe-Mg aluminous chlorite using data from phase equilibrium experiments and natural pelitic assemblages in the 100-600°C, 1-25 kbar P-T range: American Journal of Science, v. 301, p. 557–592.
Walgenwitz, F., Pagel, M., Meyer, A., Maluski, H., and Monié, P., 1990, Thermo-chronological approach to reservoir diagenesis in the offshore Angola Basin: a fluid inclusion, $^{40}Ar/^{39}Ar$ and K-Ar investigation: The American Association of Petroleum Geologists Bulletin, v. 74, 5, p. 547–563.
White, S. H., and Knipe, R. J., 1978, Transformation- and reaction-enhanced ductility in rocks: London, Journal of the Geological Society, v. 135, p. 513–516.
Wintsch, R. P., Christoffersen R., and Kronenberg, A. K., 1995, Fluid-rock reaction weakening of fault zones: Journal of Geophysical Research, v. 100, p. 13,021–13,032.